JOURNAL OF GEOPHYSICAL RESEARCH, VOL. 112, C12005, doi:10.1029/2007JC004145, 2007

A regional modeling study of the entraining Mediterranean outflow

X. Xu,[1,2] E. P. Chassignet,[3] J. F. Price,[4] T. M. Özgökmen,[1] and H. Peters[1]

Received 5 February 2007; revised 25 July 2007; accepted 5 September 2007; published 12 December 2007.

[1] We have evaluated a regional-scale simulation of the Mediterranean outflow by comparison with field data obtained in the 1988 Gulf of Cádiz Expedition. Our ocean model is based upon the Hybrid Coordinate Ocean Model (HYCOM) and includes the Richardson number–dependent entrainment parameterization of Xu et al. (2006). Given realistic topography and sufficient resolution, the model reproduces naturally the major, observed features of the Mediterranean outflow in the Gulf of Cádiz: the downstream evolution of temperature, salinity, and velocity profiles, the mean path and the spreading of the outflow plume, and most importantly, the localized, strong entrainment that has been observed to occur just west of the Strait of Gibraltar. As in all numerical solutions, there is some sensitivity to horizontal and vertical resolution. When the resolution is made coarser, the simulated currents are less vigorous and there is consequently less entrainment. Our Richardson number–dependent entrainment parameterization is therefore not recommended for direct application in coarse-resolution climate models. We have used the high-resolution regional model to investigate the response of the Mediterranean outflow to a change in the freshwater balance over the Mediterranean basin. The results are found in close agreement with the marginal sea boundary condition (MSBC): A more saline and dense Mediterranean deep water generates a significantly greater volume transport of the Mediterranean product water having only very slightly greater salinity.

Citation: Xu, X., E. P. Chassignet, J. F. Price, T. M. Özgökmen, and H. Peters (2007), A regional modeling study of the entraining Mediterranean outflow, *J. Geophys. Res.*, *112*, C12005, doi:10.1029/2007JC004145.

1. Introduction

[2] The Mediterranean Sea is a semienclosed marginal basin in which strong evaporation exceeds the sum of precipitation and river runoff, thus transforming the relatively fresh North Atlantic surface water (salinity S of 36.1) into the salty and dense Mediterranean water (S of 38.45 and potential density σ_θ of 28.95 kg m^{-3}) [*Wüst*, 1961]. As this dense water mass spreads into the North Atlantic Ocean, it mixes with the surrounding waters, creating a warm and saline tongue of water at an intermediate depth of about 1100 m that can be traced throughout the entire subtropics [*Levitus and Boyer*, 1994]. Moreover, the impact of the Mediterranean outflow water (MOW hereafter) extends well beyond the subtropics of the North Atlantic Ocean and the intermediate depth. Through either indirect or direct routes, the MOW is responsible for supplying salt to the near surface water that ultimately flows into the Nordic Seas and influences the deep water formation there [*Reid*, 1979, 1994; *Iorga and Lozier*, 1999a, 1999b; *McCartney and Mauritzen*, 2001; *Bower et al.*, 2002]. Therefore studying the Mediterranean outflow is important for understanding not only the water properties and circulation in the subsurface of the eastern North Atlantic, but also the meridional overturning circulation in the entire Atlantic basin.

[3] The circulation and evolution of the MOW begins as a bottom-trapped gravity current flowing out the Strait of Gibraltar. This dense water plume descends the Iberian continental slope, on which bottom topography, earth rotation, and bottom friction play a key role in controlling the plume pathway [*Ochoa and Bray*, 1991; *Madelain*, 1970; *Smith*, 1975; *Zenk*, 1975; *Johnson et al.*, 1994a, 1994b; *Price and Baringer*, 1994]. At the upper interface of the outflow plume, the entrainment of North Atlantic Central Water (NACW hereafter) increases the volume transport and consequently reduces the density contrast between the MOW and the ambient water [*Ambar and Howe*, 1979a, 1979b; *Baringer and Price*, 1997a, 1997b; *Price et al.*, 1993; *Zenk and Armi*, 1990]. The outflow plume shows the spatial variations and multicore features at about 7°W [e.g., *Zenk*, 1970; *Ambar and Howe*, 1979a; *Ambar*, 1983; *Ambar et al.*, 2002]. The variations have usually been attributed to

[1]Division of Meteorology and Physical Oceanography, Rosenstiel School of Marine and Atmospheric Science, University of Miami, Miami, Florida, USA.
[2]Now at Department of Marine Science, University of Southern Mississippi, Stennis Space Center, Mississippi, USA.
[3]Center for Ocean-Atmospheric Prediction Studies, Florida State University, Tallahassee, Florida, USA.
[4]Physical Oceanography Department, Woods Hole Oceanographic Institution, Woods Hole, Massachusetts, USA.

0148-0227/07/2007JC004145$09.00

differential mixing with NACW [*Baringer and Price*, 1997a, 1997b; *Iorga and Lozier*, 1999a]. An important transition in plume behavior, from a bottom-trapped density current to a wall-bounded jet, the MOW undercurrent, occurs to the west of about 8°W. Downstream from this point the plume becomes equilibrated in the water column and continues westward at intermediate depths. Further downstream at Cape St. Vincent, the bottom topography abruptly changes direction, and the flow separation from the bottom slope promotes the generation of MOW anticyclonic vortices (so-called Meddies [*McDowell and Rossby*, 1978; *Bower et al.*, 1997]). Beyond the Cape, the undercurrent generally separates into two main branches flowing northward and westward [*Daniault et al.*, 1994].

[4] Reproducing the circulation and the evolution of MOW in oceanic general circulation models (OGCMs) is a challenge. This is due not only to the high computational cost in resolving the small topographic and geographic features associated with the MOW, but also to the difficulty of accurately prescribing the entrainment process in the outflow, the key process in determining the final water properties, the volume flux, and the equilibrium depth of MOW when spreading into the North Atlantic Ocean. The difficulty of outflow representation depends strongly on the choice of vertical coordinates [*Griffies et al.*, 2000]. By construction, there is no numerically induced diapycnal mixing in isopycnic coordinate models, and the entrainment can be precisely controlled. Furthermore, these models naturally provide efficient vertical resolution by migrating isopycnals to the pycnocline atop the outflow plume.

[5] The finding by *Chang et al.* [2005], that the parameterization of *Hallberg* [2000] is too strong and the interior mixing induced by shear instability in the K-profile parameterization (KPP) [*Large et al.*, 1994, 1997] is too weak for accurately representing the entrainment process in gravity currents, led *Xu et al.* [2006] to develop a new algebraic entrainment parameterization. The parameterization casts the entrainment as a function of the layer Richardson number (Ri) times the velocity difference across layers. To determine the function $f(Ri)$, simulations of generic gravity currents over various bottom slope angles were carried out with the hydrostatic Hybrid Coordinate Ocean Model (HYCOM), and compared to similarly configured experiments using a high-resolution, three-dimensional, nonhydrostatic model, which serves as a ground truth. A simple linear function, $f(Ri) = 0.2\ (1 - Ri/0.25)$ with $Ri < 0.25$, was found to reproduce entrainment, salt flux, Richardson number, velocity profiles, and plume propagation well in comparison with the nonhydrostatic simulations. This parameterization, though extremely simple, is also consistent with the theoretical and laboratory results from stably stratified shear flows in that the shear-induced turbulence grows (decays) in the regime of $Ri < 0.25$ ($Ri > 0.25$), respectively [e.g., *Miles*, 1961; *Rohr et al.*, 1988]. When applied to a regional model of the Mediterranean outflow, the *Xu et al.* [2006] parameterization produced a better equilibrium depth of the MOW in the Gulf of Cádiz than the parameterizations of *Hallberg* [2000] and KPP.

[6] The representation of marginal sea outflows in climate models is a challenge given that climate models typically have a horizontal grid size of 1° or more. This horizontal grid spacing is one order of magnitude larger than is required to explicitly resolve the width of the narrow outflow passages. An alternative method of outflow representation in climate models was suggested by *Price and Yang* [1998] and termed the marginal sea boundary condition, or MSBC. As the name implies, the MSBC collapses the deep water formation processes (exchange between the marginal sea and the open ocean, descent and entrainment of the outflow on the continental slope) into what amounts to a side-wall boundary condition for an OGCM. This approach to modeling deep water formation by a marginal sea is appropriate from an oceanic perspective since the outflow water mass transformation takes place within one grid cell of a typical ocean climate model. In MSBC, a hydraulic model converts the surface inflow of open ocean water into an outflow source water; and a rotating, entraining density current model then transforms the source water into the final outflow product water by entraining oceanic water.

[7] This study has three aims. The first is to evaluate how well the algebraic entrainment parameterization of *Xu et al.* [2006] is able to reproduce the observed outflow when included in a well-resolved numerical, regional simulation of the Mediterranean outflow. This is achieved by performing a detailed model-data comparison, focusing on the question of whether the simulation can reproduce the localized entrainment immediately west of the Strait of the Gibraltar as well as the evolution of MOW in the Gulf of Cádiz. The second aim of this study is to investigate how sensitive this parameterization is to the horizontal and vertical resolutions used in the model. This is an important question because the regional, basin-scale, and global climate models typically use very different resolution and eddy viscosity, and will therefore have different density gradient and velocity shear, and thus Ri. The result is likely to be quite different. The third aim is to compare the HYCOM regional model and the MSBC to learn how simulated MOW product water changes when the water properties in the deep Mediterranean Sea are changed. This comparison can be regarded as an interim test for MSBC to the extent that the HYCOM simulation contains far fewer modeling assumptions. It may also be viewed as an attempt to understand/forecast the change in MOW induced by long timescale variations over the Mediterranean Sea or elsewhere in the North Atlantic Ocean; see *Curry et al.* [2003] for documented changes in salinity over the North Atlantic.

[8] The paper is organized as follows. Sections 2 and 3 briefly present the observational data and the numerical model configuration, respectively. The numerical results are compared in detail to the observations in sections 4, 5, and 6. The sensitivity of the modeled results to the horizontal and vertical resolutions is investigated in section 7. The sensitivity of the MOW product water to a water property change in outflow source water and ambient oceanic water is explored in section 8. Finally, the paper concludes with a summary and discussion.

2. Observational Data

[9] The observational data used in this study are obtained from the 1988 Gulf of Cádiz Expedition survey [*Price et al.*, 1993]. This survey primarily focused on the descent and mixing of the Mediterranean outflow as it spreads into the

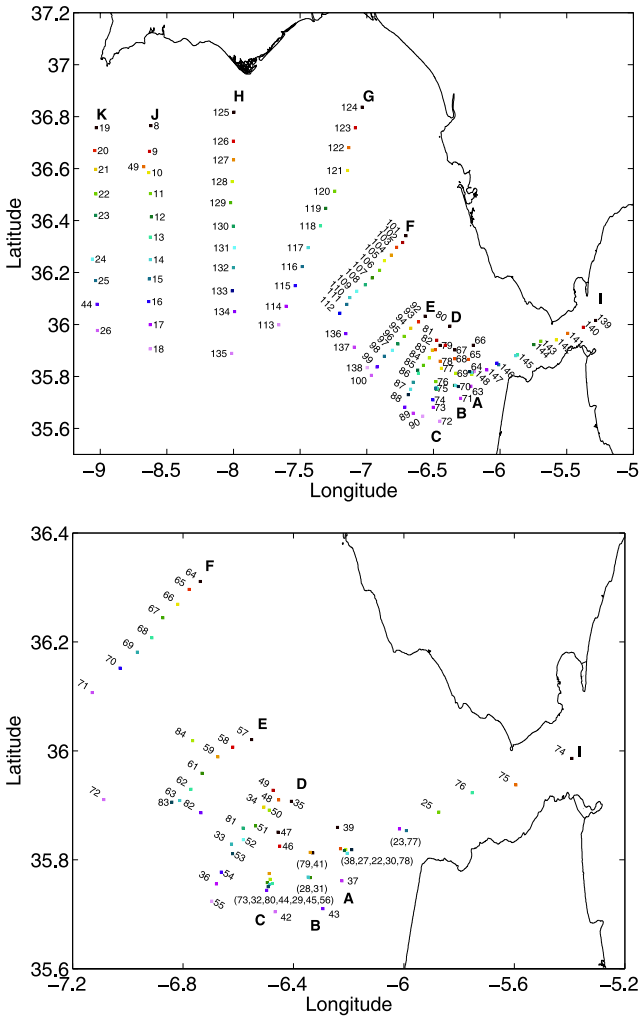

Figure 1. Locations of (top) CTD and (bottom) XCP stations during the 1988 Gulf of Cádiz Expedition.

Gulf of Cádiz, particularly the first 100 km of the path where the mixing was shown to be most intense. It therefore provides an excellent data set that can be used to evaluate our numerical simulations. The observational data that will be used in the comparison includes 120 CTD profiles and 79 in situ horizontal current profiles gathered with the XCP (expendable current profiler). Figure 1 shows the location of the stations. The CTD stations were laid out in 11 sections, labeled from A to K, with section I along the axis of the strait and the rest approximately normal to the outflow in the gulf. The XCPs were deployed throughout sections A through F whenever CTD casts indicated the presence of salty MOW. The repeat profiles in sections A, B, and C show remarkably similar velocity and density structure within the plume, implying a negligible tidal influence and a steady plume signature. Analysis of this data set has appeared in work by *Baringer* [1993], *Price et al.* [1993], *Johnson et al.* [1994a, 1994b], and *Baringer and Price* [1997a].

[10] Additional field data including mean velocity profiles obtained from measurements within the Strait of Gibraltar are used to assess the exchange between the North Atlantic and the Mediterranean. One set of velocity profiles was obtained from two moorings deployed at Gibraltar's main sill between October 1985 and October 1986 during the Gibraltar Experiment (GibEx) [*Bryden et al.*, 1994]. A second set was obtained at a nearby location during October 1994 to October 1996 with one mooring with a bottom-mounted, upward-looking Acoustic Doppler Current Profiler (ADCP), capable of measuring the velocity of the entire water column with a vertical resolution of 10 m [*Candela*, 2001].

3. Model Configuration and Exchange Through the Strait of Gibraltar

3.1. Model Configuration

[11] The general circulation model used in this study is the Hybrid Coordinate Ocean Model (HYCOM) [*Bleck*, 2002; *Chassignet et al.*, 2003; *Halliwell*, 2004]. The vertical coordinate in HYCOM is isopycnal in the open, stratified ocean and smoothly changes over to terrain-following in shallow coastal regions and to fixed depth level in the surface mixed layer and/or unstratified seas. In doing so, the model combines the advantages of different coordinate in optimally simulating coastal and open ocean circulation features. In our application, the outflow plume is primarily resolved with isopycnic coordinates.

[12] The regional model is configured with an horizontal grid resolution of 0.08° (approx. 7 km). The computational domain (13.0 ∼ 3.08°W, 34.2 ∼ 40.6°N; see Figure 2) includes the northeast Atlantic Ocean, the Gulf of Cádiz, the Strait of Gibraltar, and a small part of the western Mediterranean Sea. There are 28 layers in the vertical, with reference densities listed in Table 1. The bottom topography is based on the Naval Research Laboratory digital bathymetry database with 2-min resolution (NRL DBDB2, see http://www7320.nrlssc.navy.mil/DBDB2_WWW for documentation). The model is initialized with the temperature and salinity fields from the third version of climatology "Generalized Digital Environmental Model" (GDEM) [*Teague et al.*, 1990]. Since this is a process study, there is no surface forcing, all boundaries are closed, and relax-

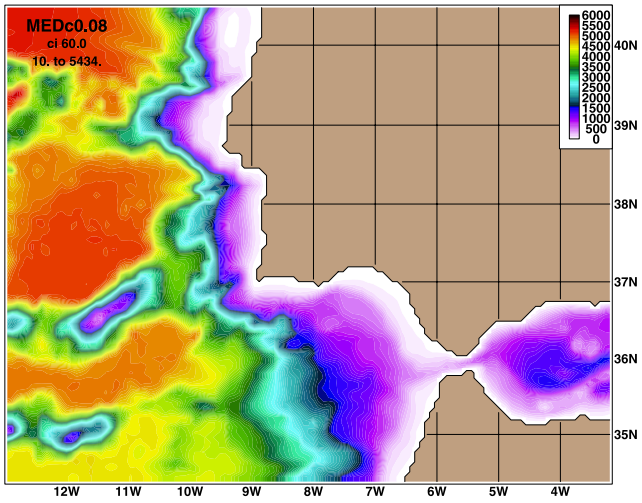

Figure 2. Bathymetry in meters of the eastern North Atlantic Ocean, the Gulf of Cádiz, and the western end of the Mediterranean Sea.

Table 1. Reference Densities $\hat{\sigma}_2$ Used in the Base Mediterranean Outflow Experiment[a]

k	$\hat{\sigma}_2$
1	23.50
2	26.00
3	27.75
4	29.25
5	30.50
6	31.75
7	32.95
8	34.01
9	34.91
10	35.45
11	35.80
12	36.04
13	36.20
14	36.38
15	36.52
16	36.62
17	36.70
18	36.77
19	36.83
20	36.89
21	36.97
22	37.02
23	37.06
24	37.10
25	37.17
26	37.30
27	37.42
28	37.48

[a]Unit is kg m^{-3}.

ation to climatology is applied near the boundaries in 1°-wide buffer zones. The simulation has a background horizontal viscosity A of $\sim$35 m^2 s^{-1} and a deformation-dependent Smagorinsky viscosity with coefficient $C = 0.1$. The bottom stress is estimated by a quadratic drag law in the lowest 10 m with a constant drag coefficient $C_D = 3.0 \times 10^{-3}$. There is small background diapycnal mixing of 10^{-5} m^2 s^{-1} and entrainment is estimated via the algebraic parameterization by *Xu et al.* [2006] noted in section 1. The model starts from rest and is integrated for 6 months.

3.2. Exchange Through the Strait of Gibraltar

[13] Unlike previous numerical studies of the Mediterranean outflow [e.g., *Jungclaus and Mellor*, 2000; *Papadakis et al.*, 2003], the model configuration used here includes part of the western Mediterranean basin and the outflow source water is supplied by relaxing the temperature and salinity fields east of 4°W (roughly 150 km to the east of the Strait) to their climatological values. The simulated vertical profiles of salinity and horizontal velocity near the Camarinal Sill (5.72°W, 35.9°N) within the Strait are therefore genuine predictions of the model, and can be compared to the velocity profiles observed at nearby locations (see Figure 3). A steady two-layer exchange flow system is quickly reached in the model, and both the salinity and velocity profiles remain nearly constant throughout the simulation. The simulated isohaline of 37.0 approximately marks the boundary between inflow and outflow, which have characteristic salinities of 36.2 and 38.45, respectively. This agrees well with the observations. The maximum outflow velocity reaches 0.5 ms^{-1}, which is about the same magnitude as reported by *Bryden et al.* [1994] but is considerably weaker than a value of about 0.8 ms^{-1} as reported by *Candela* [2001].

[14] The exchange through the Strait is often measured by a volume and/or salinity transport, and a number of estimates have been reported using different methods [see *Bryden et al.*, 1994, Table 1; *Hopkins*, 1999]. The volume transport based on evaporation and precipitation over the Mediterranean Sea ranges from 0.9 to 1.8 Sv (1 Sv = 10^6 m^3 s^{-1}) [*Hopkins*, 1978], with the most widely quoted value being 1.2 Sv [*Lacombe and Richez*, 1982]. On the basis of

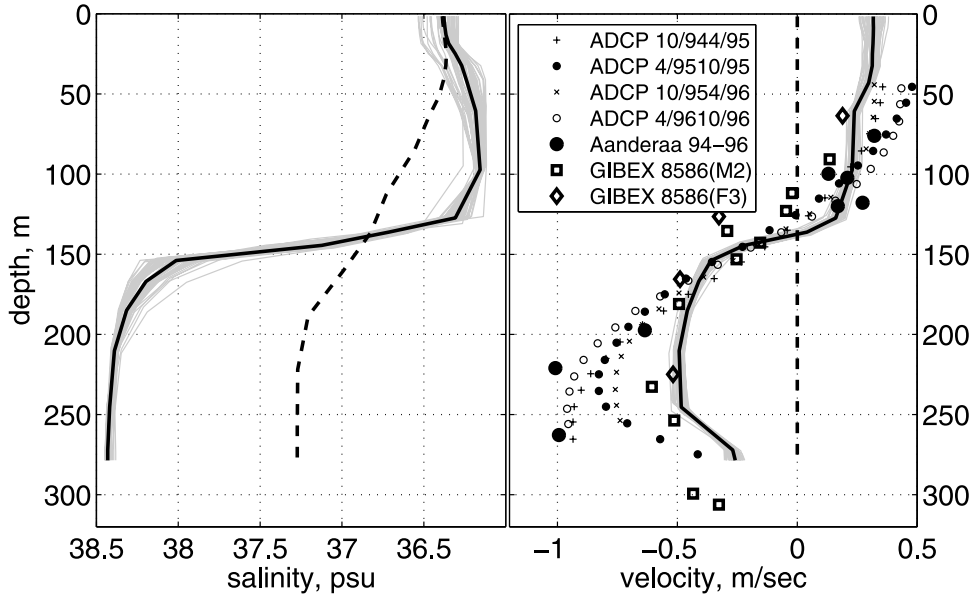

Figure 3. Simulated vertical profiles of (left) salinity and (right) horizontal velocity in the Strait of Gibraltar near the Camarinal Sill (5.72°W, 35.9°N). The thick dashed lines are the initial profiles; the thin gray lines are simulated profiles for every 3 days, and the thick solid lines represent the time-averaged profile. The observed velocity profiles are adapted from Figure 5.7.5 of *Candela* [2001].

data from GibEx, *Bryden et al.* [1994] estimate volume and salinity transports of 0.7 Sv and 1.5×10^3 m^3 s^{-1} (1×10^3 m^3 s^{-1} of salinity transport is equivalent to an inflow/outflow exchange of 1 Sv with a salinity difference of 1), respectively. *Candela* [2001] estimates a higher volume transport of 1.0 Sv which is consistent with the higher observed outflow velocity. Our numerical simulation exhibits mean values of 0.76 Sv and 1.50×10^3 m^3 s^{-1} for volume and salinity transports, respectively, in agreement with the results of GibEx.

[15] We should note here that while the model simulates the exchange through the Strait, nevertheless grid spacing does not resolve the bathymetric detail near the Strait. Thus the structure of the outflow within the Strait (e.g., the cross-sectional shape) is not well represented.

4. Characteristics of the Modeled Outflow Plume

[16] The Mediterranean outflow plume spreads into the Gulf of Cádiz through the Strait of Gibraltar as a warm, salty, dense gravity current. In this section, we examine the regional model's ability to represent the basic characteristics of the outflow plume.

4.1. T/S Profiles

[17] Figure 4 presents a direct comparison between the observed and the simulated temperature and salinity profiles in three selected CTD sections as shown in Figure 1. The model results are linearly interpolated to the location of each station and a time average of the last three months of model simulation was calculated.

[18] Immediately west of the Strait at section A, the observed outflow plume shows a two-layer structure: a weakly stratified bottom layer and a highly stratified interfacial layer above it (Figure 4a). The bottom layer has a thickness of about 60 m and maximum salinity of about 38.25. The interfacial layer, about 100 m thick, is sandwiched between the bottom layer and the NACW which is characterized by a salinity minimum of <36.0. The simulation shows a similar two-layer structure at section A. The modeled maximum salinity, however, is about 0.5 less than observed at deepest station, and somewhat more than is observed at the shallowest (northern most) station. This discrepancy is indicative of poor horizontal resolution near the Strait: 7 km grid spacing simply cannot resolve the bottom bathymetry near the Strait, where the outflow plume is observed less than 12 km wide [*Baringer*, 1993]. As the outflow plume spreads northwestward along the continental shelf of the northern Gulf of Cádiz, the weakly stratified part of the plume disappears while the plume is bottom-trapped (Figure 4b). The simulated plume at section F also shows a similar spatial salinity distribution as observed: the salinity maximum is higher in the deeper stations than in the shallower stations. Farther west at section H (about 8°W), the MOW plume detaches from the ocean floor and continues westward at depths between 1000 m and 1500 m (Figure 4c). The model successfully simulates this transition from a bottom-trapped gravity current to an interflow (or jet).

[19] The evolution of water properties of MOW in the Gulf of Cádiz is illustrated in the T-S diagram in Figure 5. The outflow begins at potential density σ_0 of ~29 kg m^{-3}, and mixes with the NACW above as the plume spreads into the Gulf of Cádiz, substantially decreasing the salinity and thus the density. When the plume is equilibrated at intermediate depth after section H, the MOW has a σ_0 value of about ~27.8 kg m^{-3}. The comparison shows that the simulation reproduces this evolution quite well.

4.2. Velocity Profiles

[20] Figure 6 presents a direct comparison between the observed and the simulated velocity profiles for three XCP sections near the exit of the Strait of Gibraltar. The same linear interpolation and time averaging process (as in T/S profiles comparison) are applied. As already mentioned, XCP data is only available in sections A to F and the repeat drops in sections A, B, and C show nearly identical velocity profiles. The simulation reproduces both the observed velocity magnitude of about 1 m s^{-1} in sections A to C and the typical vertical structure of the outflow velocity, with a maximum located between the weakly stratified bottom layer and the interfacial layer of the outflow plume. The simulation also reproduces the change in outflow plume direction from southwestward at section B to northwestward at section C. As the plume spreads farther downstream, its velocity decreases, and the simulation is overall in consistent with the observation.

5. Steering and Spreading of the Outflow Plume

[21] In the Gulf of Cádiz, we define the MOW as the water mass below the NACW with salinity $S \geq \max(S_c, S_0 + \Delta S)$, in which S_0 is the initial mean salinity profile in the gulf and $\Delta S = 0.05$ and $S_c = 36.0$. The definition is meant to 'capture' all of the newly formed MOW in the gulf. On the basis of this, the vertically averaged velocity of the MOW plume $\bar{\mathbf{u}}$ is then calculated by

$$\bar{\mathbf{u}}(x,y,t) = h^{-1} \int_D^{D+h} \mathbf{u}(x,y,z,t)\, dz\,, \tag{1}$$

in which depth D is the bottom depth of the lowest layer in model that mets the salinity criteria of MOW, and plume thickness h is the vertical summation of the thickness of MOW layers. Figure 7 shows the time average h and $\bar{\mathbf{u}}$ from the last three model months. The simulated flow bears a similar pattern to that of the schematic diagram of *Madelain* [1970]. The plume flows southwestward at the exit of the strait, where it is channel-constrained, then steers sharply to the northwest at the longitude of ~6.4°W. Part of the plume separates from the continental slope at ~7.0°W and 36.0°N moving westward. The majority of the plume, however, continues to flow northwestward along the continental slope. At about 7.6°W and 36.5°N, the plume encounters the Guadalquivir Bank which divides the flow into two branches: one flowing southwestward and the other northwestward. These two branches merge at west of 8.0°W, and the plume narrows as the steepness of the continental slope increases. The thickness h and velocity $\bar{\mathbf{u}}$ of the MOW plume from the CTD and XCP data are also plotted in Figure 7 for comparison. XCPs were taken only near the exit of the Strait where the plume steering is clearly shown. Both the simulation and the observations show a thin outflow plume (<100 m thick) when it is bottom-trapped, and the plume thickens at ~8.0°W where it becomes

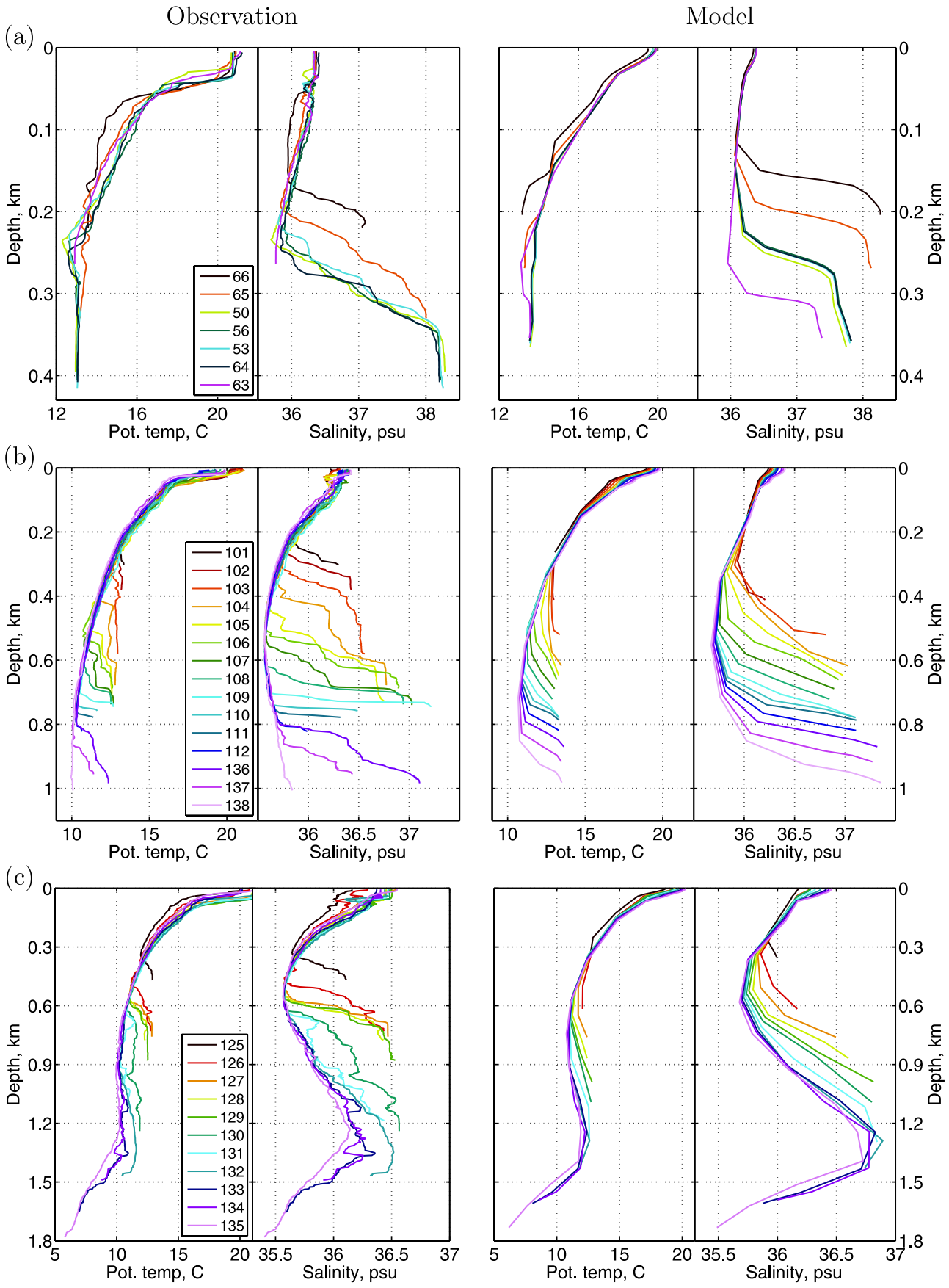

Figure 4. Comparison of T/S profiles of CTD stations between observation and model at (a) section A, (b) section F, and (c) section H.

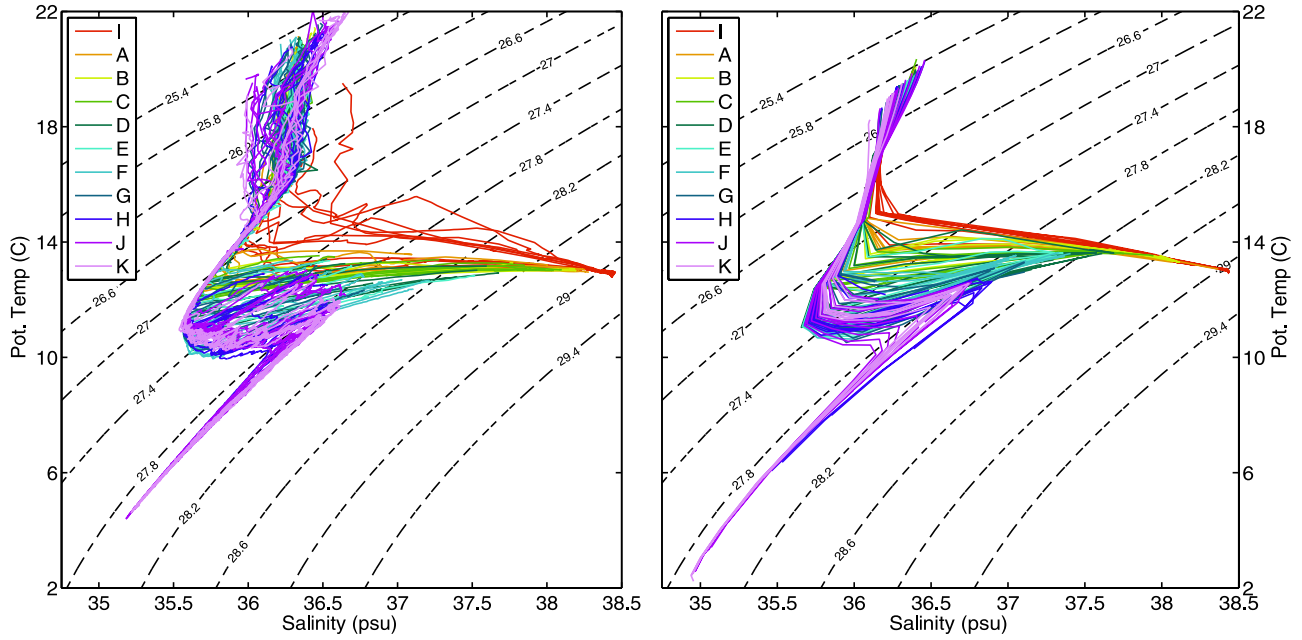

Figure 5. Comparison of T/S diagrams for all CTD sections between (left) observation and (right) model.

equilibrated at intermediate depth. However, the simulated MOW is wider and thicker than observed. West of 7°W, the simulated MOW intrudes farther south than the coverage of this survey.

[22] If the MOW plume was inviscid, it would initially accelerate down the slope driven by the strong pressure gradient, which then becomes balanced by the Coriolis force in the presence of earth rotation. The plume therefore should undergo a geostrophic adjustment which, for constant f, steers the flow direction from downslope to along the isobath. *Baringer* [1993] estimated a curvature Rossby number (the ratio of the Coriolis force to the curvature) of about 1/2, implying that inertial effects are important in the cross section momentum balance. The mechanism underneath this sharp steering is a topic of debate. *Ochoa and Bray* [1991] attribute it to the presence of a northwest-southeast ridge, but *Kenyon and Belderson* [1973] suggest that the ridge itself is depositional and is likely caused by the persistence of outflow over decades. The present simulation does not resolve the ridge owing to insufficient resolution. Nevertheless, it shows a flow direction change comparable to that observed. The steering in this simulation therefore is mainly due to the Coriolis force acting to adjust the outflow toward geostrophic balance.

[23] Because of bottom and interfacial friction, the geostrophic balance is incomplete and the plume continues to descend [*Price and Baringer*, 1994]. Furthermore, the entrainment of the NACW introduces an entrainment stress at the upper interface of the plume. A classical Ekman layer theory would predict a southward (downslope) deflection in the lower part of the plume and a northward (up-slope) deflection in the upper part. This baroclinic structure, or secondary circulation, is observed in the XCP data, from which *Baringer* [1993] estimated an ensemble mean angle of 8.6° between the averaged velocities above and below the velocity maximum. The simulation shows a similar structure (Figure 8), though with an average angle of 12.8°. This secondary circulation determines the spreading and broadening of the outflow plume, and a larger angle found in the simulation is consistent with the wider outflow plume in our simulation. This secondary circulation also tends to carry the upper and more diluted part of the outflow water inshore and the lower and less diluted part offshore, and therefore plays a role in the spatial variation of outflow T/S properties in the cross section direction.

6. Descent and Entrainment

[24] The water properties of the Mediterranean outflow plume undergo significant modifications due to the entrainment of NACW as the plume descends along the continental slope of the Gulf of Cádiz. An important feature of the entrainment process, as shown by *Baringer* [1993] and *Price and Baringer* [1994], is the strong entrainment associated with the initial steep descent of the outflow plume at about sections C and D. We next examine the distribution of entrainment in the simulation by two methods.

6.1. Downstream Evolution of Outflow Water Properties

[25] The first method consists of characterizing the entrainment process by diagnosing the downstream evolution of outflow water properties. Considering the outflow plume as a whole, we can compute the mean salinity S_{mean} and transport weighted salinity $\overline{S}$ along different meridional sections as

$$S_{mean}(x,t) = \frac{\int_0^W \int_D^{D+h} S\, dz\, dy}{\int_0^W h\, dy};$$

$$\overline{S}(x,t) = \frac{\int_0^W \int_D^{D+h} S\, u\, dz\, dy}{\int_0^W \int_D^{D+h} u\, dz\, dy}, \qquad (2)$$

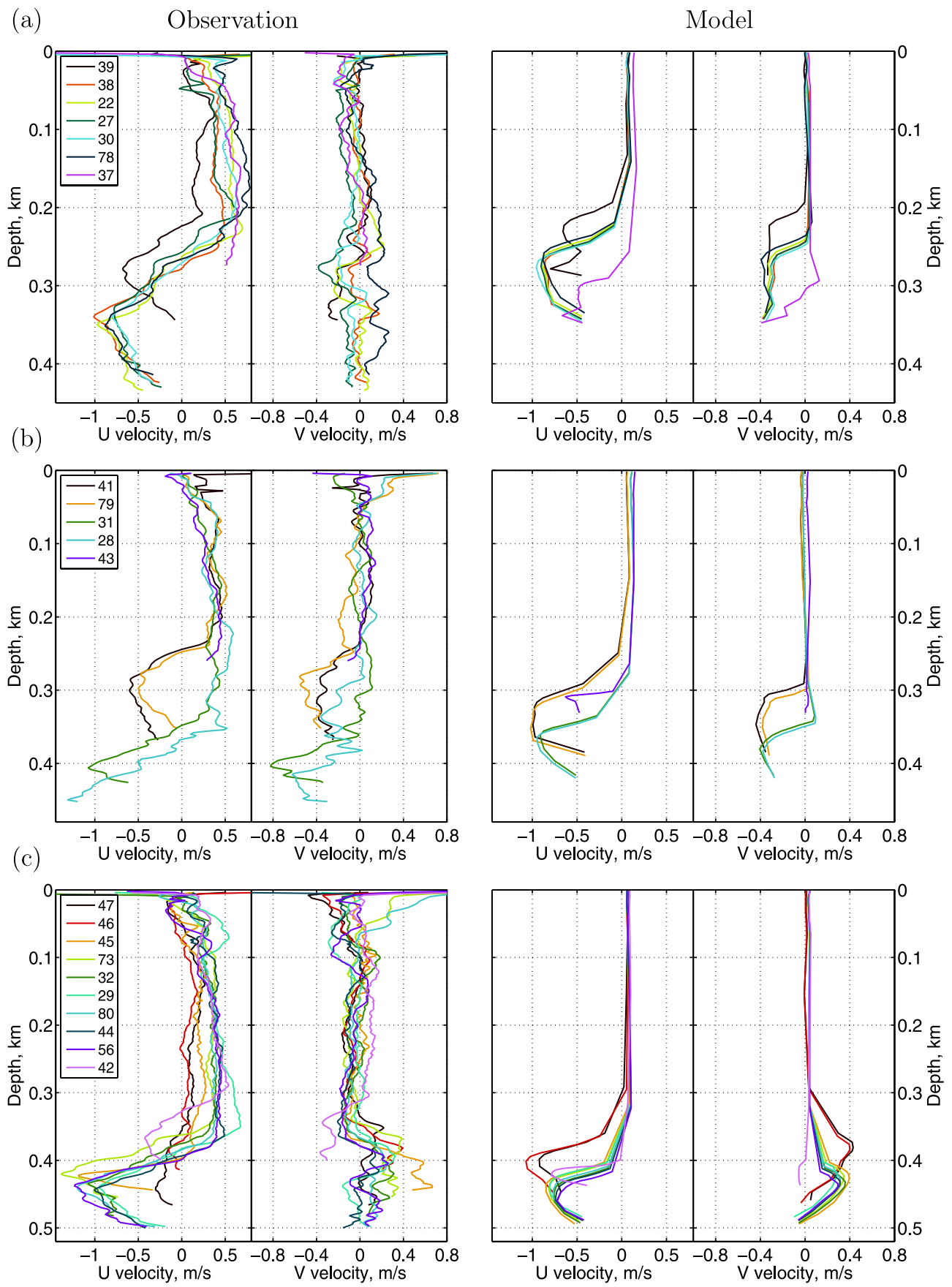

Figure 6. Comparison of U/V profiles of XCP stations between observation and model at (a) section A, (b) section B, and (c) section C.

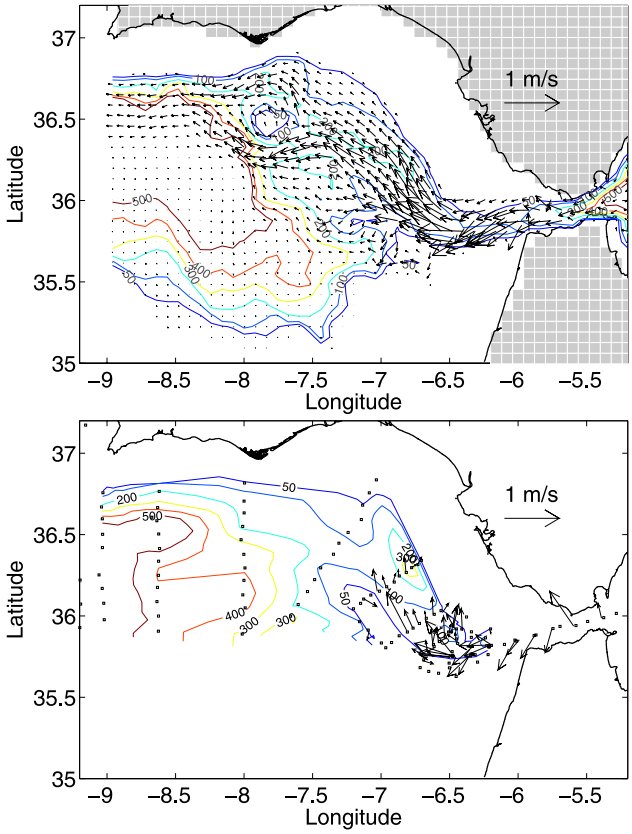

Figure 7. Horizontal structure of the (top) simulated and (bottom) observed MOW plume in the Gulf of Cádiz. The contour lines are 50, 100, 200, 300, 400, and 500 m time mean thickness; the arrows are the time-averaged and vertically averaged plume velocity.

in which W is the meridional width of the outflow plume, calculated by summing the grid space Δy meridionally whenever MOW is presented in the water column. It is also straightforward to diagnose the maximum salinity of the outflow, $S_{max}(x, t)$, and the minimum salinity of the NACW above the outflow plume, $S_{NA}(x, t)$. Figure 9a illustrates the evolution of these four simulated salinities as a function of longitude (solid lines). The observational values (dotted lines) in Figure 9a are taken from *Baringer* [1993, Table 2.3] for $\overline{S}$ and estimated from the CTD sections for S_{max}, S_{mean}, and S_{NA}.

[26] The entrainment process can be characterized as follows. First, the simulated maximum salinity of the outflow between 6.5°W and 8.0°W is significantly higher than observed. This is due to a small amount of salty water flowing slowly at the very bottom. This specific aspect of the simulation is improved by adding a bottom boundary mixing in the model (not shown here). Second and we believe most important, the simulated S_{mean} and $\overline{S}$ have very similar evolution, both decrease rapidly from 38.3 at the exit of the strait to 36.5 at ~6.8°W, and decrease slowly farther downstream. This evolution agrees with the observational results, in which the salinity decrease is most rapid east of section D. Finally, the simulated salinity is overall higher than observed. This is primarily because the climatology used as initial condition has saltier NACW above the outflow plume. The minimum salinity of NACW, which remains almost constant throughout the simulation, is about 0.1 ~ 0.2 higher than that in the observation.

6.2. Downstream Evolution of Volume Transports

[27] The second method consists of characterizing the entrainment through the downstream increase of the outflow volume transport $Q_{out}(x, t)$, defined as

$$Q_{out}(x,t) = \int_0^W \int_D^{D+h} u\, dz\, dy\,. \tag{3}$$

As shown in Figure 9b, the simulated outflow transport increases from 0.76 Sv at the strait to ~2.0 Sv at 7°W, to ~2.3 Sv at 8°W, and decreases slightly farther downstream. The simulated transport east of 7°W is higher than the observed values (the black dotted line, from Table 1 of *Baringer and Price* [1997a], in which the transport increases from 0.88 Sv at section A to 1.53 Sv at section F). While the time-mean transport of the MOW within the strait might now be regarded as fairly well known, the transport within the Gulf of Cádiz is not. Most studies indicate that the MOW transport increases by a factor of about 3 somewhere in the Gulf of Cádiz [e.g., *Ambar and Howe*, 1979b; *Ochoa and Bray*, 1991; *Rhein and Hinrichsen*, 1993]. However, exactly where and how this increase takes place is unclear. Our simulation is consistent in this respect. West of 8°W, the simulated transport decreases slightly. This is likely due to horizontal mixing with the relatively fresh water from the interior which leads to less saline waters than what is considered to be MOW.

[28] Assuming that the Mediterranean outflow source water has constant salinity, $S_{Med} = 38.44$, and the entrained NACW has the salinity of S_{NA}, we can use the conservation of mass and salt to estimate the transport of pure Mediterranean water Q_{Med} and the transport of the entrained NACW Q_{ent}:

$$\begin{aligned} Q_{out} &= Q_{Med} + Q_{ent}\,; \\ \overline{S}\, Q_{out} &= S_{Med}\, Q_{Med} + S_{NA}\, Q_{ent}\,. \end{aligned} \tag{4}$$

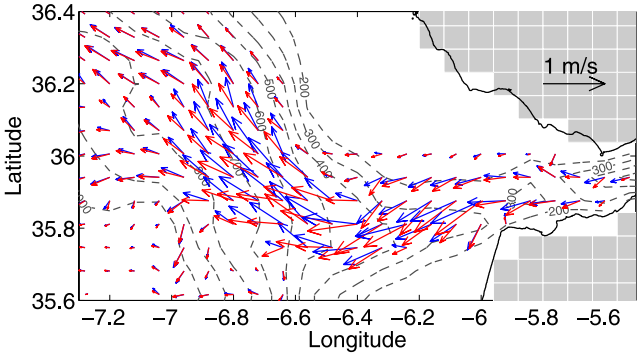

Figure 8. Averaged outflow velocity above and below the velocity maximum, represented by blue and red arrows, respectively. The contours show the isobaths increasing from 200 to 1000 m with an interval of 100 m.

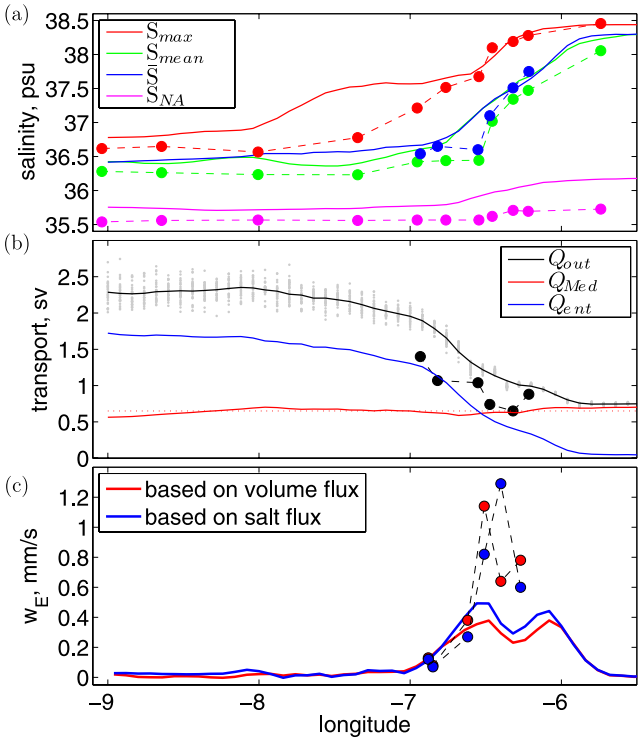

Figure 9. (a) Salinities, (b) volume transport, and (c) entrainment velocity as a function of longitude. Solid lines are from observations. In Figure 9b, the small gray dots are the $Q_{out}(x, t)$ for every 3 days and the thin red dotted line marks 0.65 Sv.

Equation (4) can be rewritten as

$$Q_{med} = \left[\frac{\overline{S} - S_{NA}}{S_{Med} - S_{NA}}\right] Q_{out}\,;$$
$$Q_{ent} = \left[\frac{S_{Med} - \overline{S}}{S_{Med} - S_{NA}}\right] Q_{out}\,. \tag{5}$$

Q_{Med} and Q_{ent} are plotted as a function of longitude in Figure 9b. The Mediterranean source water transport (red solid line), which by definition should remain a constant along longitude, is about 0.65 Sv. This indicates that the flux of pure Mediterranean water is approximately conserved per our definition of MOW. The evolution of Q_{ent} (blue solid line) is similar to that of Q_{out} since Q_{Med} varies only slightly. Consistent with the evolution of salinity, the entrainment is taking place primarily east of ~7°W (within 150 km of the strait).

6.3. Entrainment Velocity w_E

[29] From the downstream evolution of the salt flux or entrainment transport, we can estimate the entrainment velocity w_E. The equation for salinity flux integrated over a meridional cross section of the outflow plume is

$$\partial_x \int_0^W \int_D^{D+h} S\, u\, dz\, dy = -\int_0^W w_E\, S_{NA}\, dy\,. \tag{6}$$

Using the continuity equation, this can be rewritten as

$$Q_{out}\partial_x \overline{S} = \left(\overline{S} - S_{NA}\right) w_E\, W\,. \tag{7}$$

Alternatively, the entrainment velocity could be estimated directly from the evolution of entrainment transport Q_{end} alone. By definition we have

$$\partial_x Q_{ent} = w_E\, W\,. \tag{8}$$

[30] The estimated w_E is plotted in Figure 9c, in which the observed values (dotted lines) are from *Baringer and Price* [1997b]. Our estimated w_E based on salt flux (blue solid line) reaches a maximum value of ~0.5 mm s^{-1} at about 6.5°W, then decreases rapidly and remains small west of ~7.0°W. The w_E based on the entrainment transport (red solid line) is similar, but reaches slightly lower velocity maximum of ~0.4 mm s^{-1}. Overall, this localization of entrainment is consistent with the observations, in which the entrainment primarily takes place between sections C and D. The lower velocity magnitude (by a factor of 2 ~ 3) in simulation is primarily because the simulated outflow plume is wider, and the entrainment takes place over a longer distance. The end result of the entrainment process, as seen in Figures 9a and 9b, is however in good agreement with the observations. The other difference we should also note is that our w_E is based on 3-month time-averaged results, while the observation is not.

6.4. Vertical Structure of Outflow Volume Transport

[31] Additional detail of the evolution of MOW can be obtained by plotting the vertical structure of the total MOW transport through sections A to F and compared to the observations (Figure 10). For the depth and density classes, the transport is divided into bins of 20 m and 0.01 kg m^{-3}, respectively. The observations show that the outflow descends primarily between sections B and E [*Baringer and Price*, 1997a]. The simulation reproduces the overall increase of depth and decrease of density well, including that, at section D, both observation and simulation show multiple transport maxima at different depth. There are however two major differences. First, there is an eastward return flow presented in the observation at all six sections just above the outflow. The simulated return flow is much weaker at sections D and E, and totally absent at section F. This probably is associated with our model configuration, which has closed boundaries and has no surface forcing, so that the circulation in the upper ocean is not well represented. The simulated upper ocean (not shown here) contains a cyclonic gyre in the Gulf and the return flow locates almost zonally at 35.6 ~ 36°N. Second, the observations suggest that little entrainment takes place east of section A, and that the outflow water at section A is mainly the source water with a high density of 28.9 kg m^{-3}. In the simulation, however, strong entrainment has already taken place east of section A, which significantly modifies the outflow water properties.

7. Sensitivity to Horizontal and Vertical Resolutions

[32] In this section, we investigate the sensitivity of the numerical solution, especially the entrainment to horizontal

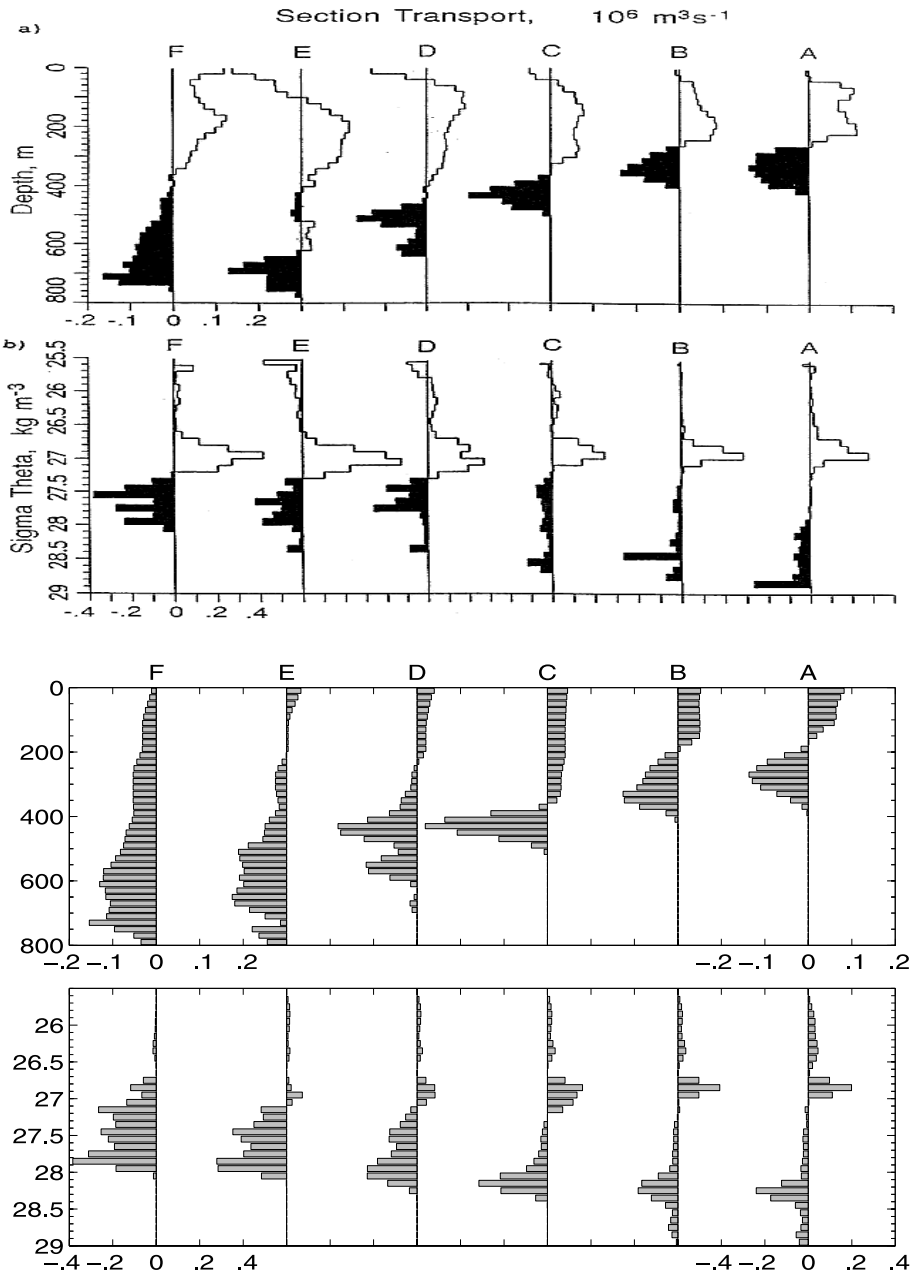

Figure 10. Volume transport of MOW (in Sv) in classes of depth (in bins of 20 m) and of potential density (in bins of 0.01 kg m^{-3}) for sections A to F. The top two plots are observations from Figure 14 of *Baringer and Price* [1997a], and the bottom two plots are from the simulation.

and vertical grid resolutions. We focus on resolution typically used in eddy-resolving and eddy-permitting configurations, i.e., 0.08°, 0.16°, and 0.32°. It is also important to realize that, associated with the horizontal resolution change, there is a corresponding change in the representation of topography. The sensitivity to the vertical resolution is investigated in the configuration with an horizontal resolution of 0.08°.

7.1. Horizontal Resolution

[33] A series of seven experiments was designed to investigate the sensitivity of the entrainment parameterization to the horizontal resolution. The configuration for all experiments is identical to the one described in section 3 (including the background diffusivity and viscosity parameters), except for the horizontal grid size and associated representation of topography. We refer to 'H1' as the reference experiment discussed in sections 4 to 6. Experiments 'H2' and 'H3', with horizontal resolution of 0.16° and 0.32°, respectively, have a bottom topography derived from averaging over the topography of experiment H1. With this choice of approach for varying resolution, the high-resolution topography features (including the coast line) of experiment H1 are filtered out and the geometry of the Strait of Gibraltar varies among three configurations (Table 2). A second approach is to start from a low-resolution configu-

Table 2. Horizontal Resolution, Width, and Sill Depth of the Strait of Gibraltar, and Volume Transport and Salinity Transport Across the Strait in Seven Experiments[a]

Experiment Number	Resolution, deg	Strait Width, km	Sill Depth, m	Volume Transport, Sv	Salinity Transport, $\times 10^3$ m^3 s^{-1}
H1	0.08	21.6 [3]	287	−0.76 ± 0.018	−1.54 ± 0.050
H1a	0.08	28.8 [4]	210	−0.77 ± 0.026	−1.52 ± 0.049
H1b	0.08	28.8 [4]	210	−0.78 ± 0.013	−1.54 ± 0.036
H2	0.16	28.8 [2]	241	−0.76 ± 0.023	−1.46 ± 0.062
H2a	0.16	28.8 [2]	210	−0.75 ± 0.029	−1.48 ± 0.058
H2b	0.16	28.8 [2]	210	−0.76 ± 0.022	−1.50 ± 0.054
H3	0.32	28.8 [1]	210	−0.75 ± 0.058	−1.43 ± 0.132

[a]The numbers in brackets are number of grids in the strait; the transports are in the form of time mean ± standard deviation.

ration and then increase the resolution so that none of the configurations contains high-resolution topographic features. There are two possible ways of treating the topography when using this approach. First, in experiments 'H2a' and 'H1a', with resolution of 0.16° and 0.08° respectively, the topography is obtained by dividing every grid box of H3 into 2 × 2 and 4 × 4 grid boxes. Second, in experiments 'H2b' and 'H1b', the topography is linearly interpolated from H3. All 7 experiments have comparable mass and salt fluxes into the Gulf of Cádiz (Table 2).

[34] Snapshots of the simulated salinity distribution in a section near 8.6°W are plotted in Figure 11 for the seven experiments. The simulated MOW in experiments H1, H2, and H3 equilibrates at depths between 1000 m and 1500 m in reasonable agreement with the observations at section J (Figure 11). The core salinity magnitude is higher than observed for the reasons laid out in section 6. In experiment H2, part of the salty MOW descends below the salinity maximum and mixes with the surrounding fresh water, leading to a thicker MOW core. The simulated MOW in experiment H3 is saltier than in H1 or H2, indicating further weakened entrainment. However, the MOW in H3 does not descend as deep as in H2 because it is also warmer. The warmer MOW is due to shallower outflow source water and shallower entrained oceanic water, both of which are associated with the topographic changes by reduction in horizontal resolution. The simulated MOW of experiments H1a and H2a equilibrates at deeper and denser isopycnals than in H3. The layer interface of H1a also shows some 'noisy jumps' separated by a distance of $2\Delta x$, where Δx is horizontal grid size. This feature highlights the importance of consistent topography representation in various resolutions. Although the topography is identical among experiments H1a, H2a, and H3, the topographic slope r, defined as $\Delta H/\Delta x$, varies significantly: r is gentle and smooth in experiment H3, yet it is 'step-like' in experiment H1a or H2a, jumping between 0 and 2 or 4 times that in H3. The experiment H1b does not exhibit the 'spurious' noise of H1a, indicating that the step topography of H1a creates the noise. Finally, when compared to H1 and H2, the simulated MOW of H1b and H2b is slightly fresher and lighter, and equilibrates at a slightly shallower depth, suggesting that small-scale topographic features affect the simulation too.

[35] The horizontal structure of the simulated MOW plume in the Gulf of Cádiz for experiments H2 and H3 is plotted in Figure 12. In comparison to Figure 7 for H1, the plume loses the detailed features of meandering, sharp steering, and splitting, owing to the lack of resolution and fine topographic details. The general pattern, however, is retained. All show a wide, thin plume in the eastern gulf merging into a narrow, thick boundary current at west of ~8°W. Although the different runs are configured with the same background viscosity parameters, the velocity of the plume becomes weaker as the resolution decreases.

[36] To quantitatively compare the plumes in the various experiments, we compute the width W, the meridionally averaged thickness $\overline{h}$, depth $\overline{D}$, and velocity $|\overline{\mathbf{u}}|$, the volume transport Q_{out}, and the salinity $\overline{S}$. The values are plotted in Figure 13 as a function of longitude. For all three horizontal resolutions, W increases from ~25 km at the strait to ~200 km at about 7.5°W, then slowly narrows to ~150 km at the western end of the gulf. Here $\overline{h}$ is nearly a constant (~100 m) between the strait and ~7.2°W, increases rapidly to ~500 m at ~8.0°W, and stabilizes farther downstream. The experiments with horizontal resolution of 0.16° have thicker MOW as already mentioned and also show considerably stronger volume transport than the corresponding 0.08° and 0.32° runs. $\overline{D}$ increases continuously from 200 m at strait to ~1000 m at 8°W, and remains at that level. The experiment H3 has a deeper equilibrium depth of MOW than the higher-resolution runs due to weaker entrainment. $|\overline{\mathbf{u}}|$ increases after the plume flows out of the strait and reaches its maximum between 6°W and 6.5°W where the plume undergoes steering, and then decreases continuously farther downstream. Between 6°W and 7°W, the magnitude of velocity decreases as the resolution decreases. The total increase of volume transport, however, remains reasonable when compared to the observations. $\overline{S}$ decreases from the strait to just east of 7°W and remains nearly a constant farther west. Overall, the entrainment weakens as the horizontal resolution decreases. This is most obvious when comparing experiments with 0.08° and 0.32°. The simulated MOW with horizontal resolutions of 0.08°, 0.16°, and 0.32°, however, all equilibrate at intermediate depths in the western part of the Gulf of Cádiz.

[37] For comparison purpose, all the experiments discussed above use the same background horizontal viscosity A of 35 m^2 s^{-1} and deformation-dependent Smagorinsky viscosity coefficient C of 0.1. However, the current practice in numerical modeling is to decrease the horizontal viscosity as the resolution is increased. Since the viscosity choice strongly influences the velocity distribution and magnitude, one may expect the mixing parameterization to be sensitive to changes in viscosity. A set of experiments with different

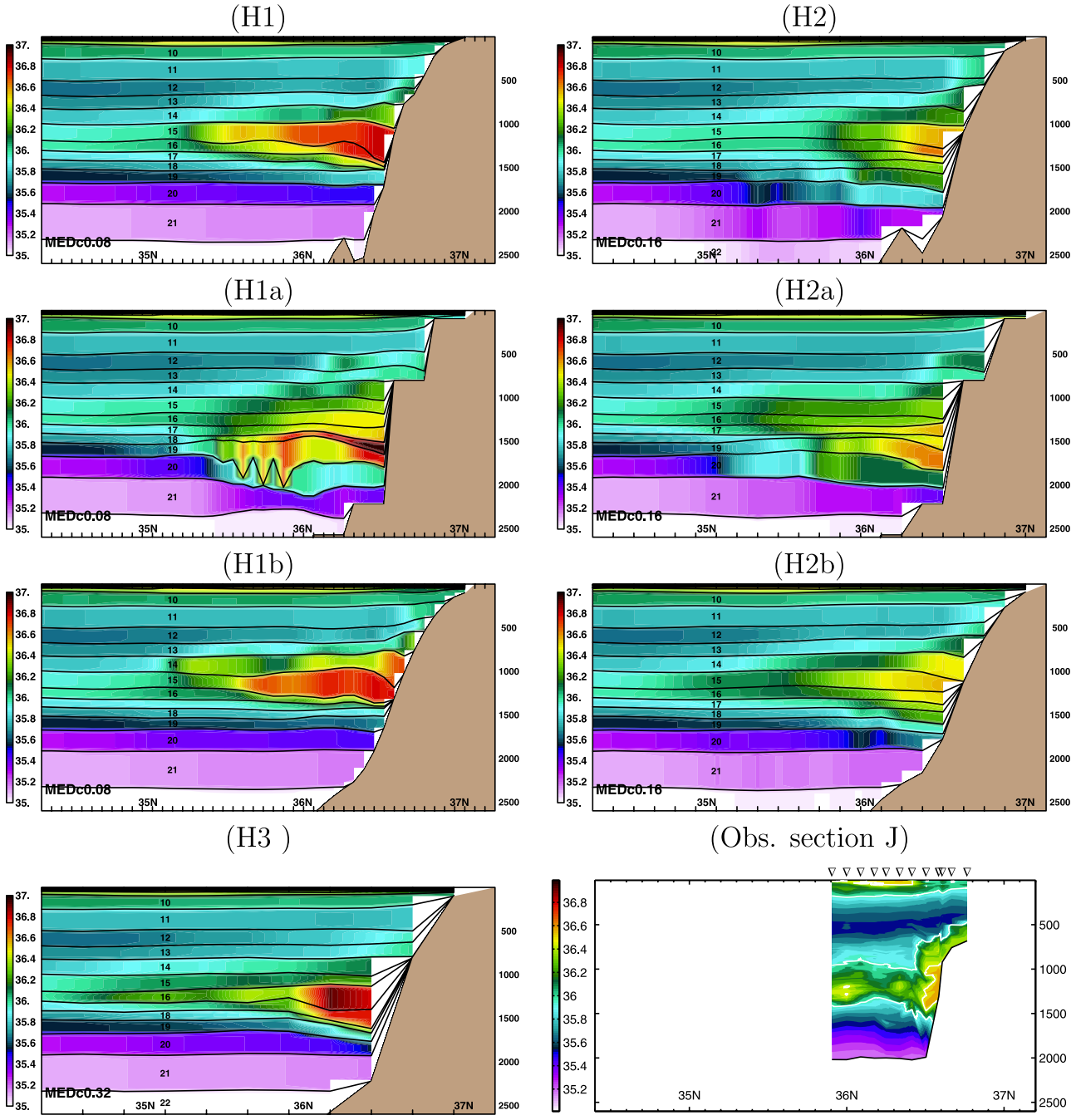

Figure 11. Snapshots of the salinity distribution near 8.6°W.

A and *C* were therefore conducted. The results (not shown) are somewhat surprising, in the sense that the simulated outflow is quite insensitive to the horizontal viscosity choices. The reason is that the entrainment primarily takes place in an area close to the strait, where the momentum balance of the outflow plume is dominated by the pressure gradients owing to the density contrast, lateral and bottom boundary stress, and Coriolis force. The eddy viscosity will however play an important role in the spreading of outflow water away from the area of strong entrainment and especially in the ocean interior.

7.2. Sensitivity to Vertical Resolution

[38] We now examine how sensitive the entrainment parameterization under different vertical grid resolutions. The Mediterranean outflow product water is equilibrated at layer 16 ($\hat{\sigma}_2$ = 36.62 kg m^{-3}). For the entrainment parameterization, vertical resolution is therefore needed between layer 16 and the bottom. The number of layers below layer 16 was varied in four experiments with the same horizontal resolution of 0.08° (see Figure 14): 13-layer (including layer 16) is the reference experiment, a slightly

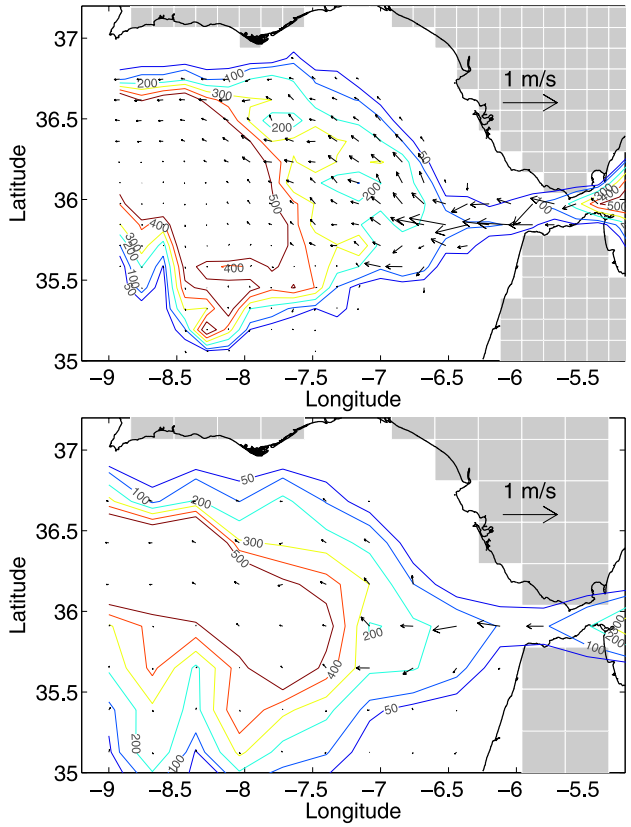

Figure 12. As in Figure 7, but for experiments (top) H2 and (bottom) H3.

higher resolution experiment has 15 layers, and two coarser resolution experiments have 7 and 4 layers, respectively.

[39] Salinity snapshots at 8.6° W from these four experiments are plotted in Figure 15. The two high vertical resolution configurations of 13 and 15 layers lead to very similar results, suggesting that the numerical results are robust for the reference vertical resolution. The entrainment is reduced in the seven-layer experiment and the simulated MOW is deeper and mixes with the less saline waters located underneath the salinity maximum. The experiment with four layers is even worse in the sense that part of the MOW descends to the very bottom of the ocean and that MOW is present in the entire water column below 1000 m. One therefore needs a minimum vertical resolution (on the order of 10 layers between the Mediterranean outflow source and the final product water) in order for the entrainment parameterization to work. This is not surprising, since the vertical resolution is the key factor that influences the model's skill to resolve the shear Richardson number *Ri*.

8. MOW in a Changing Climate

[40] From the results presented in the previous section, it is clear that the parameterized entrainment will become even weaker when using grid sizes of 1° or more, a resolution which is typically used in climate models. *Price and Yang* [1998] proposed the marginal sea boundary condition (MSBC) as an alternative method to an explicit outflow representation in coarse resolution climate models. In this section, we investigate, by comparing the HYCOM regional model and the MSBC, the sensitivity of MOW to an imposed water property change in the Mediterranean Sea or in the Gulf of Cádiz.

8.1. Experimental Setup

[41] Typical vertical profiles of the T, S, and density ρ in the Mediterranean Sea and the Gulf of Cádiz are illustrated in Figure 16. Dynamically, the most important quantity is the density contrast between the two basins evaluated at the sill depth in the Strait of Gibraltar. It has a value of $\Delta\rho \approx 2.0$ kg m^{-3} in the reference case. Two sets of HYCOM experiments are designed. The first set contains source water change: T, S, and ρ fields in the Gulf of Cádiz are the same as in the reference experiment. In the Mediterranean Sea, T is also the same as in the reference experiment, while ρ is shifted by a spatially uniform value, ±10% and ±20% of $\Delta\rho$. S is then calculated from The second set contains oceanic water change: T, S, and ρ fields in the Mediterranean Sea are the same as in the reference experiment. In the Gulf of Cádiz, T is also the same as in the reference experiment, while ρ is shifted by the same spatially uniform values noted above and S is then calculated from ρ and T.

[42] The MSBC model equations are given by *Price and Yang* [1998]. The T/S profiles in the Gulf of Cádiz for the HYCOM are very similar to the profiles of *Price and Yang* [1998] (Figure 16). In order to make the reference states of

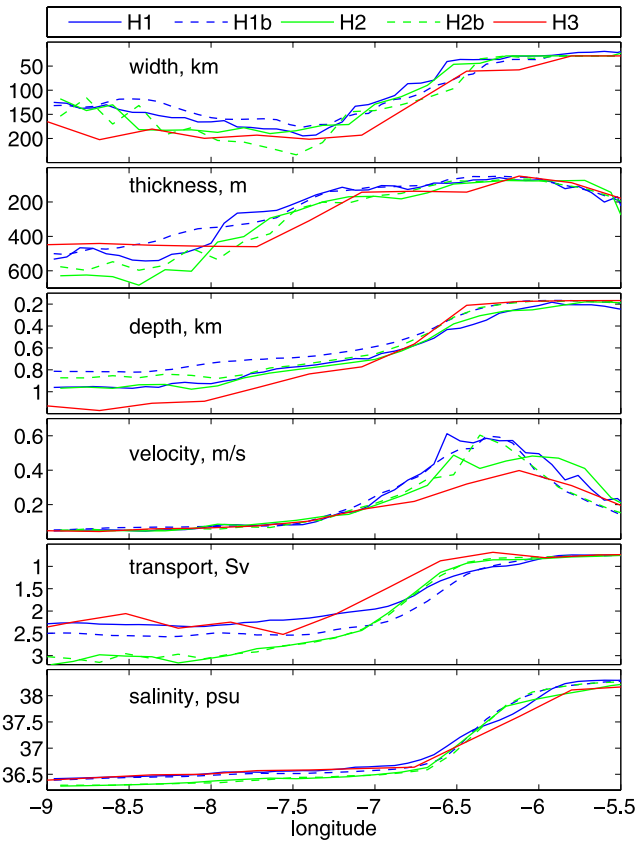

Figure 13. Width W, thickness $\overline{h}$, depth $\overline{D}$, velocity $\overline{u}$, volume transport Q_{out}, and salinity $\overline{S}$ of the simulated outflow plume as a function of longitude.

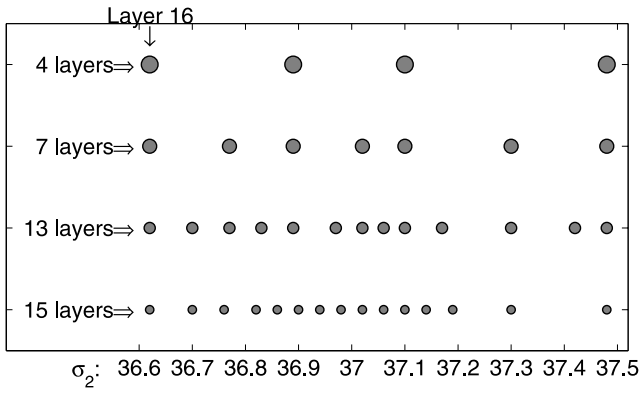

Figure 14. Distribution of target density ($\hat{\sigma}_2$) between 36.62 and 37.48 kg m^{-3} in four configurations.

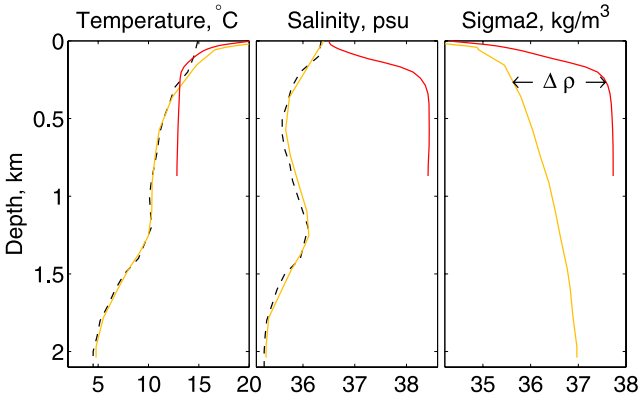

Figure 16. T(z), S(z), and $\rho(z)$ in the Mediterranean Sea (red) and in the Gulf of Cádiz (orange) from the reference experiment. $\Delta\rho$ = 2 kg m^{-3} marks the reference density contrast between the two basins. The black dash lines show the ocean profiles from *Price and Yang* [1998].

the MSBC and HYCOM nearly identical, we have made changes to three of the independent, geophysical variables that have to be provided to the MSBC (see Table 3). In the MSBC, the Mediterranean source water properties are the result of prescribed air-sea heat and fresh water flux over the Mediterranean basin and exchange with the North Atlantic. *Price and Yang* [1998] ignored the small but not quite negligible heat flux over the Mediterranean basin, of about 5–10 W m^{-2} as inferred from the heat budget of the Mediterranean basin. Variable fluxes (an E–P of 0.35 ∼ 0.75 m a^{-1} and a heat flux of −6.0 ∼ −7.6 W m^{-2}) are specified in order to have outflow source water from MSBC that is closely consistent with that from HYCOM. Also, *Price and Yang* [1998] took the depth of entrainment to be 400 m, which is on the upper side of the depth range over which the Mediterranean outflow entrains, roughly 400 m to 700 m judging from the HYCOM regional model. We have here set the entrainment depth to be 600 m. Clearly then, the reference state of the MSBC is the result of some modest tuning, and is not fully (or blindly) predicted. This is likely true of every ocean model solution if one construes parameter tuning and model configuration to be the ends of a continuum, model development. The issue is whether the chosen values or model configurations are within a plausible range, and we believe that they are for both HYCOM and MSBC. However, the reference state is not the central issue here, because our intent is to examine the sensitivity of product water transport to source water density, say, which is only slightly dependent upon the reference state of the models. This sensitivity is almost entirely due to model dynamics and is thus a genuine prediction of the models.

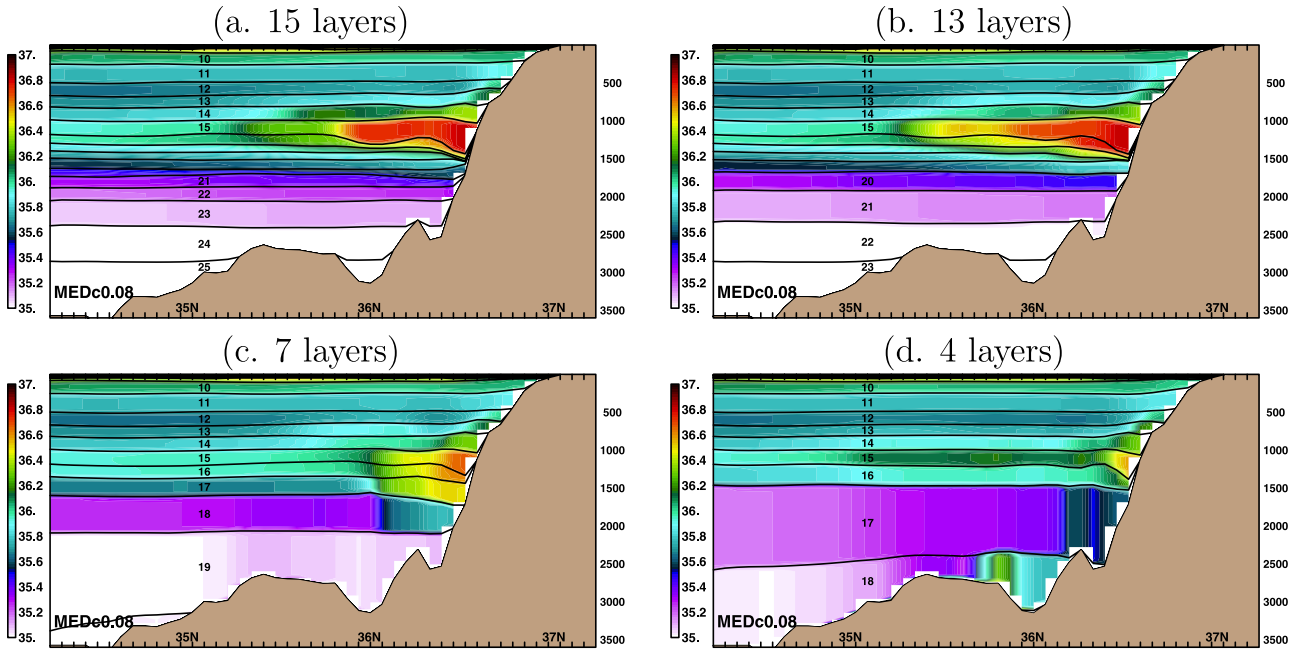

Figure 15. Snapshots of the salinity distribution at a meridional section at 9° with different number of layers between the outflow source water and product water.

Table 3. Parameters of the MSBC for the Mediterranean Outflow[a]

	ϕ, deg	W, km	d_s, m	A, $\times 10^6$ km^2	Q, W m^{-2}	E−P m a^{-1}	α	d_e, m
PY98	36	20	300	2.5	0	0.7	0.012	400
Here	-	-	-	-	−6.0 ∼ −7.6	0.35 ∼ 0.75	-	600

[a]Entries ϕ, W, and d_s are the latitude, width, and sill depth of the Strait of Gibraltar; A, Q, and E−P are the area, the heat flux (negative indicates heat loss from the marginal sea), and the evaporation minus precipitation of the Mediterranean Sea; α is the continental slope; d_e is the depth at which entrainment takes place; and a dash means no change with respect to work by *Price and Yang* [1998].

8.2. Imposed Source Water Change

[43] The snapshots of the salinity distribution at a meridional section in the Gulf of Cádiz (8.6°W) from HYCOM are presented in Figures 17a and 17c. As the density (and salinity) of the outflow source water increases, a larger amount of the Mediterranean outflow water is introduced into the gulf. The product water has a slightly higher value of maximum salinity and equilibrates at slightly denser and deeper isopycnic layers.

[44] The volume transport Q, salinity $\overline{S}$, temperature $\overline{T}$, and depth $\overline{D}$ of the outflow plume are calculated following the definition of the MOW as in section 5. These quantities are zonally averaged between longitude 6° ∼ 5.5°W and 9° ∼ 8°W for the source and product water masses, respectively. Finally, time averaging is applied to determine mean properties in HYCOM. A comparison of HYCOM and MSBC solutions under conditions of different source water densities is presented in Figure 18. Overall, the MSBC and HYCOM indicate comparable variations of the source and product water transports, and T/S (density). As the outflow source water becomes saltier and denser, the increased density contrast significantly increases the amount of entrainment, and thus the volume transport of the product water. The variation in product water salinity is thus virtually eliminated via increased entrainment. The variations of the temperature and depth is also in good agreement between MSBC and HYCOM results.

8.3. Imposed Oceanic Water Changes

[45] The snapshots of the salinity distribution from HYCOM experiments with oceanic water change are shown in Figures 17b and 17d. Compared to Figures 17a and 17c, the outflow salinity in the Gulf of Cádiz varies much more. The magnitude of the variation (∼1) is nearly the same as that of the oceanic water change. As the oceanic water becomes saltier (and denser), the simulated MOW equilibrates in denser isopycnic layers but at slightly shallower depths.

[46] To be consistent with the varying oceanic water profiles, the constant S_c is shifted by −0.53, −0.265, 0.265, and 0.53 in defining the MOW in the four sensitivity experiments. The comparison between HYCOM and MSBC is summarized in Figure 19. The increase of density in the oceanic water reduces the density contrast between the outflow source water and the oceanic water, and this leads to weaker entrainment and thus a smaller volume transport of outflow product water. Weaker entrainment means less dilution of the outflow. Since the outflow begins with the same source water properties, the salinity of the outflow product water varies much more than in the previous scenario of imposed source water change. Overall, the comparison shows similar trends in the outflow product water between HYCOM and MSBC.

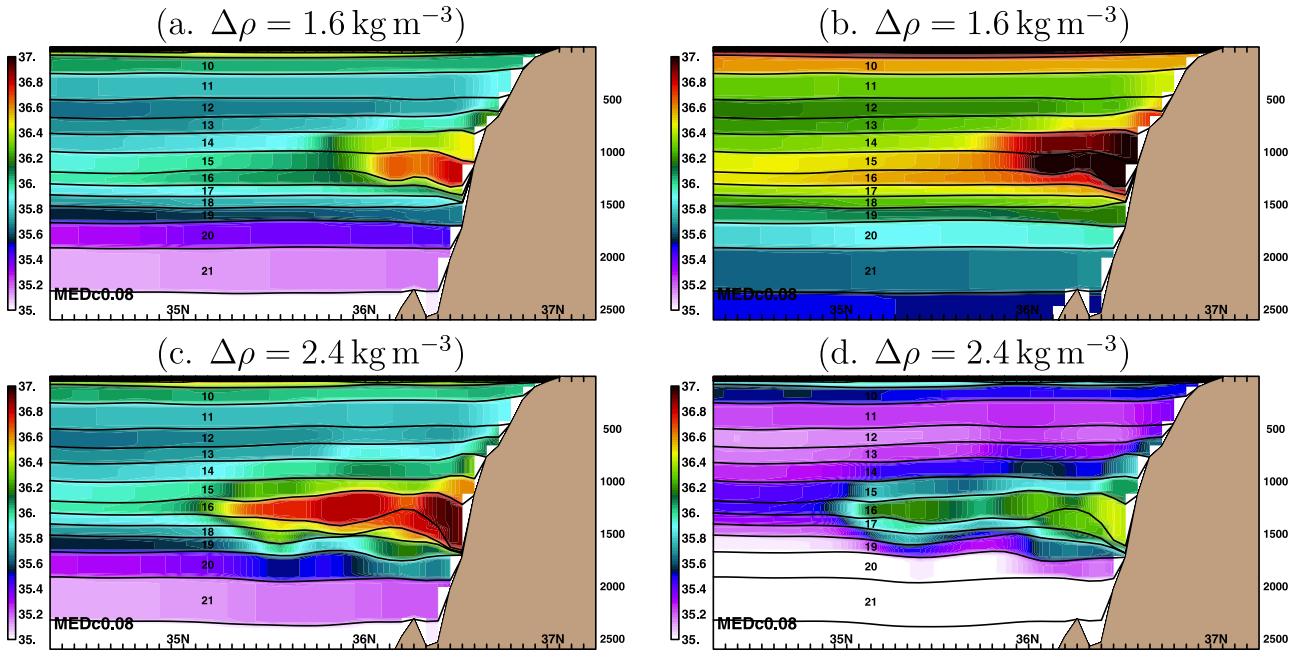

Figure 17. Snapshots of salinity distribution at 8.6°W calculated by HYCOM in five experiments with different density contrasts. (a, c) Cases with outflow source water changes. (b, d) Cases with ambient ocean water changes.

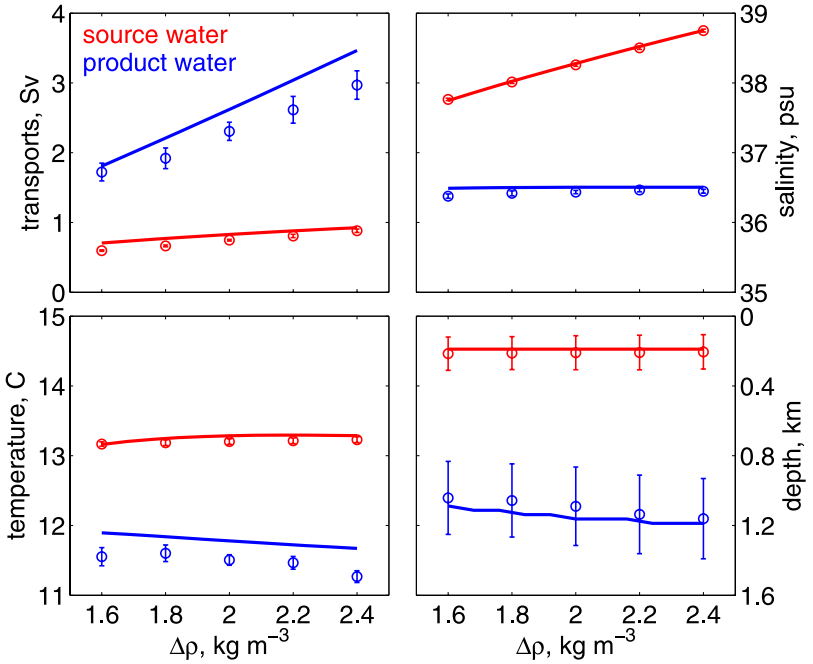

Figure 18. Results from MSBC versus HYCOM in the case of outflow source water change. Lines are from MSBC, and circles are the HYCOM results. Error bars represent the standard deviation for transport, salinity, and temperature, and the mean upper and lower interface of outflow plume for depth in HYCOM results. The red and blue colors represent the outflow source and product waters, respectively.

[47] To quantify the variations in the outflow product water properties relative to changes in outflow source water and oceanic water, we define four non-dimensional quantities, $(\frac{\Delta\rho}{Q_p})\frac{dQ_p}{d\Delta\rho}$, $(\frac{\Delta\rho}{S_p})\frac{dS_p}{d\Delta\rho}$, $(\frac{\Delta\rho}{T_p})\frac{dT_p}{d\Delta\rho}$, $(\frac{\Delta\rho}{D_p})\frac{dD_p}{d\Delta\rho}$, where Q_p, S_p, T_p, and D_p are volume transport, salinity, temperature, and equilibrium depth of the outflow product water (Table 4). These quantities can be interpreted as the variation, normalized by their reference values, induced by the variation of density contrast. The most pronounced result, as already predicted by MSBC, is that the volume transport of the

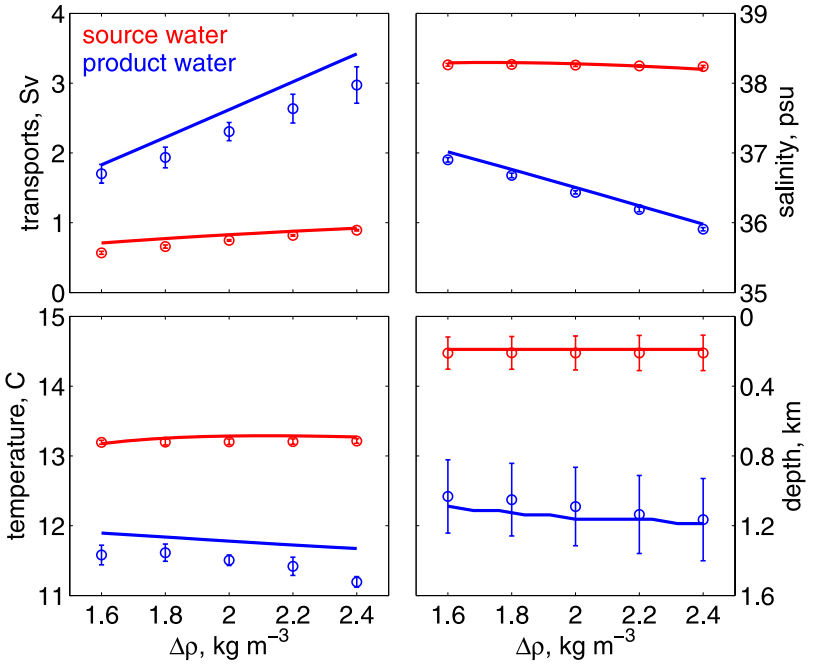

Figure 19. As in Figure 18, but for experiments in which the ocean water was changed. Note that the transport, temperature, and equilibration depth shown here are very similar to those found in Figure 18. The salinity difference between source and product water is also similar to Figure 18.

Table 4. Normalized Derivatives in Cases of Outflow Source Water Change and Ocean Water Change[a]

	$(\Delta\rho/Q_p)\ dQ_p/d(\Delta\rho)$	$(\Delta\rho/S_p)\ dS_p/d(\Delta\rho)$	$(\Delta\rho/T_p)\ dT_p/d(\Delta\rho)$	$(\Delta\rho/D_p)\ dD_p/d(\Delta\rho)$
Outflow source water change	1.352 [1.577]	0.005 [0.001]	−0.062 [−0.047]	0.272 [0.215]
Ocean water change	1.376 [1.516]	−0.068 [−0.071]	−0.084 [−0.047]	0.304 [0.215]

[a]Numbers in brackets show MSBC results, and the others are HYCOM results.

outflow product water is equally sensitive to $\Delta\rho$ variation caused either by the source water or the oceanic water. The salinity, however, is at least 1 order more sensitive to changing oceanic water than to changing source water. The comparison between the HYCOM regional simulation and MSBC suggests that the MSBC, as simple as it is, captures the main outflow dynamics and produces comparable outflow variations due to a change either in the Mediterranean Sea or in the Gulf of Cádiz. It therefore holds some promise for coarse horizontal resolution climate models in which representing these variations are of great importance.

9. Summary and Discussion

[48] The performance of the entrainment parameterization of *Xu et al.* [2006] was evaluated in a series of realistic Mediterranean outflow experiments using a regional HYCOM configuration with horizontal resolution of 0.08°. The model is forced by the density contrast between the North Atlantic Ocean and the Mediterranean sea, which drives a surprisingly (given the minimally resolved Strait) realistic exchange flow through the Strait of Gibraltar. Comparison to the field data obtained in the 1988 Gulf of Cádiz Expedition shows that the simulation reproduces naturally several important features of the observed Mediterranean outflow in the Gulf of Cádiz, including the evolution of temperature, salinity and velocity profiles, the steering and spreading of the outflow plume as it descends along the continental slope, and most importantly, the localized entrainment immediately west of the strait where the outflow water experiences a significant modification in both volume transport and water properties. One important aspect of MOW our simulation did not capture well is the mesoscale variability, and the simulated MOW appears quite steady. Experiments with better boundary condition, finer resolution, and longer time integration would be helpful in understanding this. We should also note that the bottom friction plays an important role in the outflow dynamics too. It would be interesting to explore the sensitivity of a simulated MOW to bottom stress parameters.

[49] The results are, however, sensitive to the horizontal grid resolution choices. The entrainment weakens as the grid spacing increases, i.e., higher-resolution simulations tend to show stronger entrainment than the lower resolution cases. This is consistent with the observation that the flow is generally weaker in the lower resolution simulations, leading to higher Richardson numbers and thus to less mixing (entrainment). Our results also emphasize the importance of the topography representation in simulating outflows. Because outflows are bottom-trapped plumes that flow across the isobaths, they directly 'feel' the details of the topography. The high resolution experiment with large step-like topography that mimics the coarser resolution experiment shows significantly deeper and denser Mediterranean outflow water, as well as spurious 'noise' due to the discontinuous topographic variation. The details of the simulated MOW also differ between experiments with and without the high-resolution topographic features, indicating that they play an important role in the outflow representation as well. Proper vertical resolution is also needed for a correct representation of the entrainment process. Insufficient vertical resolution leads to weaker entrainment and to a deeper intrusion of the Mediterranean outflow water. In the extreme case of only four layers between the Mediterranean outflow source and product water, the present Richardson number–dependent parameterization that works with high resolution fails almost completely, and the resulting MOW alters the water column from 1000 m to the bottom. Most ocean climate models do not resolve the Richardson number and therefore cannot use the *Ri*-dependent parameterization of *Xu et al.* [2006].

[50] An alternative approach to the explicit outflow representation is suggested by *Price and Yang* [1998] and termed the marginal sea boundary condition, or MSBC. The MSBC collapses the deep water formation processes into what amounts to a side-wall boundary condition for an OGCM. The sensitivity of the simulated MOW to imposed water property changes in the Mediterranean Sea and in the Gulf of Cádiz is compared between the HYCOM regional model and the MSBC. The comparison suggests that while the MSBC does not resolve any detailed aspects of the outflow plume, it does reproduce closely comparable variations of outflow product water associated with changes in both the outflows source water and the oceanic water. In particular, both models show that (1) changes in the oceanic water lead to significant changes in the product water salinity, while comparable changes in the source water produce little change in the product water salinity (the sensitivity, measured by the logarithmic derivative, differs by a factor of about 10 or more); and (2) the volume transport of the outflow product water is about equally sensitive to a change in the density contrast brought about by changing the source water or the oceanic water. Of all the things that might influence the sensitivity of an outflow to the ocean environment, evidently the ones included in the MSBC (nearly geostrophic velocities, Froude number closure of the entrainment process, and the steepest (but still moderate in large scale) topography) are the ones that count the most in the present context. To close, we want to point out that this study has considered only the most obvious effects of a marginal sea outflow, namely the transport and T/S of the product water that enters the open ocean. These also happen to be the only things that the present MSBC deals with. The substantial cross-stream variation of the real Mediterranean outflow is missed altogether by the MSBC, but is predicted by HYCOM; the potential vorticity flux [*Özgökmen et al.*, 2001; *Kida*, 2006] associated with an

outflow is more imposed than predicted by the MSBC but is, again, predicted by HYCOM. If we knew these aspects of outflow dynamics as well as we think we know the gross transport and T/S properties, and if they are found to be important in climate-scale ocean models, then they might perhaps be added to a future MSBC.

[51] **Acknowledgments.** We are grateful for the support of National Science Foundation via grant OCE0336799 and of the National Ocean Partnership Program (NOPP) via award N000140410676. The authors benefited greatly from discussions with the other PIs of the Climate Process Team on Entrainment in Gravity Currents. J. H. Dunlap and T. B. Sanford from the University of Washington have kindly provided the preprocessed data of the 1988 Gulf of Cádiz Expedition. We thank the two anonymous reviewers for their constructive comments and suggestions, which greatly improved the manuscript.

References

Ambar, I. (1983), A shallow core of Mediterranean water off western Portugal, *Deep Sea Res.*, *30*, 677–680.

Ambar, I., and M. R. Howe (1979a), Observations of the Mediterranean outflow. I. Mixing in the Mediterranean outflow, *Deep Sea Res., Part A*, *26*, 535–554.

Ambar, I., and M. R. Howe (1979b), Observations of the Mediterranean outflow. II. The deep circulation in the vicinity of the Gulf of Cadiz, *Deep Sea Res., Part A*, *26*, 555–568.

Ambar, I., N. Serra, M. J. Brogueira, G. Cabeçadas, F. Abrantes, P. Freitas, C. Gonçalves, and N. Gonzalez (2002), Physical, chemical and sedimentological aspects of the Mediterranean outflow off Iberia, *Deep Sea Res., Part II*, *49*, 4163–4177.

Baringer, M. O. (1993), Mixing and dynamics of the Mediterranean outflow, *WHOI-93-52*, 244 pp, Woods Hole Oceanogr. Inst., Woods Hole, Mass.

Baringer, M. O., and J. F. Price (1997a), Mixing and spreading of the Mediterranean outflow, *J. Phys. Oceanogr.*, *27*, 1654–1677.

Baringer, M. O., and J. F. Price (1997b), Momentum and energy balance of the Mediterranean outflow, *J. Phys. Oceanogr.*, *27*, 1678–1692.

Bleck, R. (2002), An oceanic general circulation model framed in hybrid isopycnic-Cartesian coordinates, *Ocean Modell.*, *37*, 55–88.

Bower, A. S., L. Armi, and I. Ambar (1997), Lagrangian observations of meddy formation during a Mediterranean Undercurrent seeding experiment, *J. Phys. Oceanogr.*, *27*, 2545–2575.

Bower, A. S., B. L. Cann, T. Rossby, W. Zenk, J. Gould, K. Speer, P. L. Richardson, M. D. Prater, and H.-M. Zhang (2002), Directly measured mid-depth circulation in the northeastern North Atlantic Ocean, *Nature*, *419*, 603–607.

Bryden, H. L., J. C. Candela, and T. H. Kinder (1994), Exchange through the Strait of Gibraltar, *Prog. Oceanogr.*, *33*, 201–248.

Candela, J. (2001), Mediterranean water and global circulation, in *Ocean Circulation and Climate*, edited by G. Siedler, J. Church, and J. Gould, pp. 419–429, Academic Press, San Diego, Calif.

Chang, Y., X. Xu, T. Özgökmen, E. P. Chassignet, H. Peters, and P. F. Fischer (2005), Comparison of gravity current mixing parameterizations and calibration using a high-resolution 3D nonhydrostatic spectral element model, *Ocean Modell.*, *10*, 342–368.

Chassignet, E. P., L. T. Smith, G. R. Halliwell, and R. Bleck (2003), North Atlantic simulations with the hybrid coordinate ocean model (HYCOM): Impact of the vertical coordinate choice, reference pressure, and thermobaricity, *J. Phys. Oceanogr.*, *33*, 2504–2526.

Curry, R. G., R. R. Dickson, and I. Yashayaev (2003), A change in the freshwater balance of the Atlantic Ocean over the past four decades, *Nature*, *426*, 826–829.

Daniault, N., J. P. Maze, and M. Arhan (1994), Circulation and mixing of Mediterranean water west of the Iberian Peninsula, *Deep Sea Res., Part I*, *41*, 1685–1714.

Griffies, S. M., C. Böning, F. O. Bryan, E. P. Chassignet, R. Gerdes, H. Hasumi, A. Hirst, A.-M. Treguier, and D. Webb (2000), Developments in ocean climate modelling, *Ocean Modell.*, *2*, 123–192.

Hallberg, R. (2000), Time integration of diapycnal diffusion and Richardson number dependent mixing in isopycnal coordinate ocean models, *Mon. Weather Rev.*, *128*, 1402–1419.

Halliwell, G. R. (2004), Evaluation of vertical coordinate and vertical mixing algorithms in the HYbrid-Coorinate Ocean Model (HYCOM), *Ocean Modell.*, *7*, 285–322.

Hopkins, T. S. (1978), Physical processes in the Mediterranean basins, in *Estuarine Transport Processes*, edited by B. Kjerve, pp. 269–310, Univ. of S. C. Press, Columbia.

Hopkins, T. S. (1999), The thermohaline forcing of the Gibraltar exchange, *J. Mar. Syst.*, *20*, 1–31.

Iorga, M. C., and M. S. Lozier (1999a), Signatures of the Mediterranean outflow from a North Atlantic climatology: 1. Salinity and density fields, *J. Geophys. Res.*, *104*, 25,985–26,009.

Iorga, M. C., and M. S. Lozier (1999b), Signatures of the Mediterranean outflow from a North Atlantic climatology: 2. Diagnostic velocity fields, *J. Geophys. Res.*, *104*, 26,011–26,029.

Johnson, G. C., R. G. Lueck, and M. O. Baringer (1994a), Stress on the Mediterranean outflow plume. Part II: Turbulent dissipation and shear measurement, *J. Phys. Oceanogr.*, *24*, 2084–2092.

Johnson, G. C., T. B. Sanford, and M. O. Baringer (1994b), Stress on the Mediterranean outflow plume. Part I: Velocity and water property measurement, *J. Phys. Oceanogr.*, *24*, 2072–2083.

Jungclaus, J. H., and G. Mellor (2000), A three-dimensional model study of the Meditarranean outflow, *J. Mar. Syst.*, *24*, 41–66.

Kenyon, N. H., and R. H. Belderson (1973), Bed forms of the Mediterranean undercurrent observed with side-scan sonar, *Sediment. Geol.*, *9*, 77–99.

Kida, S. (2006), Overflows and upper ocean interaction: A mechanism for the Azores Current, Ph.D. thesis, Mass. Inst. of Technol./Woods Hole Oceanogr. Inst. Joint Program, Woods Hole.

Lacombe, H., and C. Richez (1982), The regime of the strait of Gibraltar, in *Hydrodynamics of Semi-Enclosed Seas*, *Oceanogr. Ser.*, vol. 34, edited by J. C. J. Nihoul, pp. 13–73, Elsevier, New York.

Large, W. G., J. C. McWilliams, and S. C. Doney (1994), Ocean vertical mixing: A review and a model with a nonlocal boundary layer parameterization, *Rev. Geophys.*, *32*, 363–403.

Large, W. G., G. Danabasoglu, S. C. Doney, and J. C. McWilliams (1997), Sensitivity to surface forcing and boundary layer mixing in a global ocean model: Annual-mean climatology, *J. Phys. Oceanogr.*, *27*, 2418–2447.

Levitus, S., and T. Boyer (1994), *World Ocean Atlas 1994*, vol. 4, *Temperature, NOAA Atlas NESDIS 4*, 129 pp., NOAA, Silver Spring, Md.

Madelain, F. (1970), Influence de la topographie du fond sur l'ecoulement Mediterranee entre le Detroit de Gebraltar et le Cap Saint-Vincent, *Cah. Oceanogr.*, *22*, 43–61.

McCartney, M. S., and C. Mauritzen (2001), On the origin of the warm infow to the Nordic Seas, *Prog. Oceanogr.*, *51*, 125–214.

McDowell, S. E., and H. T. Rossby (1978), Mediterranean water: An intense mesoscale eddy off the Bahamas, *Science*, *202*, 1085–1087.

Miles, J. W. (1961), On the stability of heterogeneous shear flows, *J. Fluid Mech.*, *10*, 496–508.

Ochoa, J., and N. A. Bray (1991), Water mass exchange in the Gulf of Cadiz, *Deep Sea Res.*, *38*, S465–S503, suppl. 1.

Özgökmen, T. M., E. Chassignet, and C. H. Rooth (2001), On the connection between the Mediterranean outflow and the Azores Current, *J. Phys. Oceanogr.*, *31*, 461–480.

Papadakis, M. P., E. P. Chassignet, and R. W. Hallberg (2003), Numerical simulations of the Mediterranean Sea outflow: Impact of the entrainment parameterization in an isopycnic coordinate model, *Ocean Modell.*, *5*, 325–356.

Price, J. F., and M. O. Baringer (1994), Outflows and deep water production by marginal seas, *Prog. Oceanogr.*, *33*, 161–200.

Price, J. F., and J. Yang (1998), Marginal sea overflows for climate simulations, in *Ocean Modelling and Parameterization*, edited by E. Chassignet and J. Verron, pp. 155–170, Kluwer Acad., Norwell, Mass.

Price, J. F., M. O. Baringer, R. G. Lueck, G. C. Johnson, I. Ambar, G. Parrilla, A. Cantos, M. A. Kennelly, and T. B. Sanford (1993), Mediterranean outflows and dynamics, *Science*, *259*, 1277–1282.

Reid, J. L. (1979), On the contribution of the Mediterranean Sea outflow to the Norwegian-Greenland Sea, *Deep Sea Res., Part A*, *26*, 1199–1223.

Reid, J. L. (1994), On the total geostrophic circulation of the North Atlantic Ocean, *Prog. Oceanogr.*, *33*, 1–99.

Rhein, M., and H. H. Hinrichsen (1993), Modification of Mediterranean water in the Gulf of Cadiz, studied with hydrographic, nutrient and chlorofluoromethane data, *Deep Sea Res., Part I*, *40*, 267–291.

Rohr, J. J., E. C. Itsweire, K. N. Helland, and C. V. Atta (1988), Growth and decay of turbulence in stably stratified shear flow, *J. Fluid Mech.*, *195*, 77–111.

Smith, P. C. (1975), A streamtube model for bottom boundary currents in the ocean, *Deep Sea Res.*, *22*, 853–873.

Teague, W. J., M. J. Carron, and P. J. Hogan (1990), A comparison between the Generalized Digital Environmental Model and Levitus climatologies, *J. Geophys. Res.*, *95*, 7167–7183.

Wüst, G. (1961), On the vertical circulation of the Mediterranean Sea, *J. Geophys. Res.*, *66*, 3261–3271.

Xu, X., Y. S. Chang, H. Peters, T. M. Özgökmen, and E. P. Chassignet (2006), Parameterization of gravity current entrainment for ocean circula-

tion models using a high-order 3D nonhydrostatic spectral element model, *Ocean Modell.*, *14*, 19–44.
Zenk, W. (1970), On the temperature and salinity structure of the Mediterranean Water in the North Atlantic, *Deep Sea Res.*, *17*, 627–631.
Zenk, W. (1975), On the Mediterranean Outflow west of Gibraltar, *Meteor Forschungsergeb. A*, *16*, 23–34.
Zenk, W., and L. Armi (1990), The complex spreading pattern of Mediterranean water off the Portuguese slope, *Deep Sea Res.*, *37*, 1805–2392.

E. P. Chassignet, Center for Ocean-Atmospheric Prediction Studies, Florida State University, 200 R. M. Johnson Building, 2035 East Paul Dirac Drive, P.O. Box 3062840, Tallahassee, FL 32306-2840, USA. (echassignet@coaps.fsu.edu)

T. M. Özgökmen and H. Peters, Division of Meteorology and Physical Oceanography, Rosenstiel School of Marine and Atmospheric Science, University of Miami, Miami, FL, USA. (tozgokmen@rsmas.miami.edu; hpeters@rsmas.miami.edu)

J. F. Price, Physical Oceanography Department, Woods Hole Oceanographic Institution, MS 29, Clark 209, Woods Hole, MA 02543, USA. (jprice@whoi.edu)

X. Xu, Department of Marine Science, University of Southern Mississippi, 1020 Balch Boulevard, Stennis Space Center, MS 39529, USA. (xiaobiao.xu@usm.edu)